PHYSICAL MODELLING OF TAILINGS DAM BREACH

by

Andrea Rae Walsh

A thesis submitted to the Department of Civil Engineering

In conformity with the requirements for

the degree of Master of Applied Science

Queen's University

Kingston, Ontario, Canada

(December, 2019)

Abstract

Tailings dams are constructed in stages, exhibit sediment deposits located in the reservoir upstream of the dam crest (beaches) generated from slurry deposition, and are commonly designed with shallower upstream slopes in contrast with conventional water storage dams. Current breach models for the failure mode of overtopping, used to inform flood routing and emergency preparedness plans, have been developed for water storage dams and have not been calibrated to the tailings dam case. This thesis presents the results of eleven 1m high homogeneous fine sand dams brought to failure by overtopping to investigate the influence of dam geometries varying from water storage dams to tailings dams on the outflow hydrograph. Laboratory observations indicate that the breach crest geometry can be described as a semi-ellipse, and that the size and shape of the breach crest controls instantaneous discharge during breach. This geometric relationship, coupled with an observed linear breach crest growth rate and a discharge equation were shown to permit an estimation of discharge from the onset of breach to peak discharge. Peak discharge was demonstrated to occur when the combination of breach crest length and depth of water flowing over the crest were at their maximum, given a finite reservoir volume. The reservoir storage function was shown to limit breach discharge when the reservoir elevation fell below the sum of the dam height below the breach crest location and maximum potential depth of water flowing over the breach crest. These findings enabled calculation of the maximum discharge rate and time to reach peak discharge, based on reservoir and dam upstream geometry. The presence of a shallowly sloping beach in the reservoir impacted peak discharge only in the case where the beach was intersected by the breach crest while the discharge rate was on the rising limb of the outflow hydrograph. A reduction in peak discharge was observed in tests where the beach height was greater than this threshold, including scenarios that resulted in an approximately 50% reduction in peak discharge rate.

Acknowledgements

They say many hands make light work. I'm not so sure that's true, but there are many people who were instrumental in making this project possible. To my supervisor, Dr. Andy Take, thank you for taking me on at the start of this new research program. Your passion for big science is infectious and your positivity radiates through the whole group. I am so excited to watch the story unfold in the years to come.

Support for this work was also provided by our CanBreach (Canadian Tailings Dam Breach Research) project partners: Dr. Scott McDougall (University of British Columbia), Dr. Stephen G. Evans (University of Waterloo), Imperial Oil Resources Inc., Suncor Energy Inc., BGC Engineering Inc., Klohn Crippen Berger, Golder Associates Ltd., and the Natural Sciences and Engineering Research Council of Canada.

To the Civil Engineering Department staff, especially Graeme Boyd, Josh Coghlan, and Hal Stephens, thank you for fostering such a great lab environment and helping to bring my project to life.

Thanks to the old Ellis 101 gang: Gemma, Liam, Ramy, Scott, Eric and Ray, for showing me the ropes early on. To Geo-Fit™ members: Erica, Meg, Sam, Ruobing, Alex, Wolfe, Natalie, and Branna, thank you for sweating in the sandbox with me. I very literally could not have run any experiments without your help.

To the incredible people I'm fortunate enough to call my friends, thank you for supporting me in so many ways. Special thanks to Clare, Jess, Keith, and Soph, for letting me impose on your living rooms during these last few months of writing. I hope I can return the favour sometime.

To my family, thank you for encouraging me to pursue anything I've been interested in and to always do my best. To my mom, Arleen, my first role model and motivator to stay on the academic path, thanks for the help when I needed it most.

And to Bob, I cannot adequately put into words how appreciative I am for your love and patience throughout this degree. From across the country or across the border, you have been a consistent light in my life and made it all seem possible in (the many) times of doubt.

Table of Contents

List of Figures

List of Tables

Chapter 1

Introduction

1.1 Tailings Dams

1.1.1 Tailings Generation and Storage

During the ore recovery process, mined materials are generally ground at a processing mill for mineral extraction. The waste byproduct created during this process is referred to as tailings. To comply with environmental regulations, this waste material is stored at the mine site, often contained by constructed dams, also termed tailings storage facilities (TSFs)

The grain size of tailings is dependent on site specific conditions and requirements for mineral extraction, but commonly ranges from sand to clay size fractions (Engels, 2006). A common method to transport tailings from the mill to the TSF is via a slurry pipeline, where the slurry is discharged subaerially via a spigot. This deposition method can lead to the formation of a shallowly sloping beach, between the embankment and supernatant pond (Ritcey, 1989). Coarser, heavier grains drop out of slurry suspension close to the discharge point, while finer grained material is transported further upstream of the discharge point (McPhail, 1994) (Figure 1.1). The tailings beach may form part of the embankment structure as the dam is raised throughout the life of mine.

The three principal classes of raised tailings dam construction, designated by the direction the embankment crests moves with respect to the starter dyke, include: upstream, centerline and downstream (Vick, 1983) (Figure 1.2). The upstream method requires the smallest footprint and is typically the least costly. However, this method does not include internal drainage zones, and relies on coarse grained material in the beach to dissipate pore water pressures and prevent saturation of the embankment structure. Hence, the upstream method is not amenable to areas with high seismic

activity or rapid increases in pond elevation, and loading from embankment raises must be carefully controlled to limit the risk of liquefaction (Davies et al., 2002)

1.1.2 Tailings Dam Breach and Dam Safety Guidelines

Tailings dam breach is failure of a dam structure resulting in the uncontrolled release of retained materials in a sudden or catastrophic manner (Martin et al., 2019). The Canadian Dam Association (CDA) Dam Safety Guidelines addresses failure analysis and assessment requirements for both water retaining and tailings dams, needed to classify the dam hazard rating and to develop emergency response plans in the case of failure (CDA, 2007). However, tailings dams differ from water retaining dams in a number of ways including (but not limited to): extended construction durations, type of material being retained, and design geometry. The CDA Dam Safety Guidelines offer little in terms of standardized and comprehensive methods to conduct dam breach assessments specific to tailings dams. Practioners are currently reliant on a combination of other guidance documents, published papers and professional judgement to perform this work (Martin et al., 2015).

1.2 Research Need

Recent notable examples of tailings dam breach include: Mount Polly in 2014 in British Columbia, Canada, Fundão in Minas Gerais, Brazil in 2015 (Figure 1.3), Cadia in New South Wales, Australia in 2018, and the breach at Córrego do Feijao in Brumadinho, Brazil in 2019. Failure at this high rate of occurrence and level of consequence is not tolerated in general engineering practice (Saiyar et al., 2019). Tailings dam design and operations need to be improved to lower the probability of failure and to better manage the risk associated with dam failure. Regulatory bodies globally been creating and updating guidelines in reaction to these failures, including recent resolutions by the Brazilian government to ban construction by the upstream method, a precaution that has been instituted in seismically-active Chile since 1970 (Morrison & Gomide, 2019). To effectively manage risk from tailings dam breach, the failure process, and how it may differ from water

retaining dams, must be better understood. However, there is a scarcity of data available to improve the state of practice. More research efforts are required to quantify dam breach processes specific to tailings dams for a variety of failure modes.

1.3 Previous Work

There are several methods established to conduct breach analysis, including parametric models based on empirical data, and physically based models which combine hydraulic, structural and geotechnical properties to numerically predict the breaching process (West et al., 2018).

Empirical models for tailings dam breach typically predict peak discharge, outflow volume and runout distance as a function of dam height and volume retained (e.g. Rico et al., 2008; Rourke & Luppnow, 2015; Small et al., 2017 Larrauri & Lall, 2018). Such relations currently include a high degree of uncertainty due to the small number of cases available with sufficient datasets.

Limited research has been conducted to inform physically based models for the tailings case. However, large scale physical modelling of water retaining dams has been an active research topic, providing valuable details on the breach processes observed. Recent efforts have produced seminal data, resulting in improved breach modelling abilities, including work at the University of Auckland by Coleman et al. 2002, the IMPACT project by Morris et al. 2007, the United States Department of Agriculture – Agricultural Research Service (USDA-ARS) Hydraulic Unit by Hanson et al. 2005, University of Ottawa by Al-Riffai & Nistor 2010, United States Geological Survey (USGS) by Walder et al. 2015 (Figure 1.4), and the Laboratório Nacional de Engenharia Civil (LNEC) in Portugal by Amaral et al. 2019.

Observations of the breach crest shape by Coleman et al. 2002, on noncohesive, homogenous dams breached by overtopping, described it as a curved (hourglass) shape in plan view. The breach crest was defined by connecting a series of high points along streamlines flowing over the breach channel where flow is perpendicular to the breach crest at all points along its length. The geometry of the

breach crest was defined by breach width, B^*, the horizontal distance between the two ends of the breach crest, and breach arc length, B, measuring the curvilinear distance along the arc shape (Figure 1.5). In contrast to common methods where the breach crest is thought of a trapezoidal shaped gutter, formed in balance between erosional and depositional processes, Walder et al. 2015 demonstrated the curved breach crest is a purely erosional feature, functioning as an upstream hydraulic control structure, analogous to a weir.

1.4 Research Objectives

Dam breach models, developed for water retaining structures, have not yet been calibrated for the tailings dam case, in large part due to the lack of available data. The overall goal of this research project was to explore how breach evolution may differ for tailings dams, and to quantify these impacts in terms of the breach outflow hydrograph. A large-scale physical model program was undertaken which, for the first time, included upstream geometry conditions that are typical of tailings dams. The specific objectives of this research are to:

- Investigate the effect of dam upstream slope angle on peak discharge for water retaining dams, whilst capturing high-resolution measurements of the evolving geometry of the upstream breach crest to observe and quantify the breach crest's control on instantaneous outflow;
- Evaluate the scenario in which breach occurs in a dam with tailings-style beaches in the upstream reservoir; in particular, to quantify under which conditions the peak outflow rate is influenced by the presence of a beach.

1.5 Methods

These objectives were achieved by conducting two separate series of physical model dam breach experiments to quantify peak discharge under a variety of geometries and to monitor breach crest

evolution. All tests were performed at the Queen's University Coastal Engineering Laboratory in the large landslide flume. Each breach was initiated by incising a v-notch in the dam crest, which resulted in overtopping failure.

The first test series included six 1.0 m high dams, with upstream slope angles ranging from 10.0° to 30.0° from horizontal. A downstream slope inclination of 3H:1V, or 18.4°, and dam crest width of 0.30 m was maintained for all tests.

The second test series included five 1.0 m high dams, each with a dam upstream slope angle of 18.4°. Shallowly sloping beaches were constructed upstream of these dams, intersecting the dam upstream slope at elevations ranging from 0.50 m to 0.90 m. The downstream dam geometry and crest width were the same as the previous test series.

1.6 Organization of the Thesis

This thesis is presented in manuscript format as outlined by the School of Graduate Studies at Queen's University. Chapter 1 is a general introduction, Chapters 2 and 3 present draft manuscripts, and Chapter 4 gives an overall summary of the work and general conclusions.

Chapter 2, "*Effect of reservoir and upstream dam geometry on peak discharge during overtopping breach in noncohesive homogenous embankment dams"*, examines the influence of upstream slope angle on peak discharge during breach of a water retaining dam.

Chapter 3, *"Effect of beach elevation on peak discharge observed during overtopping of physical model tailings dams"*, quantifies how a shallowly sloping tailings beach may reduce peak discharge in certain cases.

Chapter 4 discusses the overall findings of this research project, presents conclusions and highlights areas for future research.

1.7 References

Al-Riffai, M., & Nistor, I. (2010). Impact and analysis of geotechnical processes on earthfill dam breaching. *Natural Hazards*, *55*(1), 15–27. https://doi.org/10.1007/s11069-010-9586-6

Amaral, S., Alvarez, T., Caldeira, L., Viseu, T., & Ferreira, R. M. L. (2019). Recent advances on experimental dam breach studies. *Mecânica Experimental*, *31*(November), 11–25.

Canadian Dam Association (CDA). (2007). Revised 2013. *Dam Safety Guidelines*.

Coleman, S. E., Andrews, D. P., & Webby, M. G. (2002). Overtopping breaching of noncohesive homogeneous embankments. *Journal of Hydraulic Engineering*, *128*(9), 829–838. https://doi.org/10.1061/(ASCE)0733-9429(2002)128:9(829)

Davies, M., McRoberts, E., & Martin, T. E. (2002). Static liquefaction of tailings: fundamentals and case histories. *Tailing Dams 2002: Association of State Dam Safety Officials, U.S. Society on Dams, April 29-May 1, 2002, Orleans Hotel, Las Vegas, Nevada*.

Engels, J. (2006). *An Expert Management System for Surface Tailings Storage* (University of Leeds). Retrieved from http://www.tailings.info/basics/tailings.htm

Hanson, G. J., Cook, K. R., & Hunt, S. L. (2005). Physical Modelling of Overtopping Erosion and Breach Formation of Cohesive Embankments. *Transactions of the ASCE*, *48*(5), 1783–1794.

Larrauri, P. C., & Lall, U. (2018). Tailings Dams Failures: Updated Statistical Model for Discharge Volume and Runout. *Environments*, *5*(2), 28. https://doi.org/10.3390/environments5020028

Martin, V., Al-Mamun, M., & Small, A. (2019). CDA technical bulletin on tailings dam breach analyses. *Sustainable and Safe Dams Around the World*, *d*, 3484–3498. https://doi.org/10.1201/9780429319778-313

Martin, Violeta, Fontaine, D., & Cathcart, J. (2015). Challenges with conducting tailings dam

breach studies. *Proceedings of Tailings and Mine Waste 2015 Conference*, 314–328.

McPhail, G. (1994). *Prediction of the Beaching Characteristics of Hydraulicaly Placed Tailings*. University of Witwatersrand, Johannesburg, South Africa.

Morris, M. W., Hassan, M. A. A. M., & Vaskinn, K. A. (2007). Breach formation: Field test and laboratory experiments. *Journal of Hydraulic Research*, *45*(SPEC. ISS.), 9–17. https://doi.org/10.1080/00221686.2007.9521828

Morrison, K. F., & Gomide, P. C. R. (2019). Post-Córrego do Feijão : Continued Evolution of Tailings Dam Regulations in Brazil. In J. Goodwill, D. Van Zyl, & M. Davies (Eds.), *Proceedings of Tailings and Mine Waste Conference 2019* (pp. 391–400). Vancouver, British Columbia.

Ritcey, G. M. (1989). *Tailings management : problems and solutions in the mining industry*. Elsevier.

Rourke, H., & Luppnow, D. (2015). The risks of excess water on tailings facilities and its application to dam-break studies. *Tailings and Mine Waste Management for the 21st Century*, (July), 225–230.

Saiyar, M., Ryans, M., & Becker, D. E. (2019). Review of Recent Significant Tailings Dam Failures and Their Influence on Dam Safety Management. *Proceedings of 2019 CDA Annual Conference*. Calgary, Alberta.

Small, A., James, M., & Al-mamun, M. (2017). Advancing the State of Practice for Tailings Dam Breach Assessment Using Empirical Correlations. *Proceedings of 2017 CDA Annual Conference*. Kelown, British Columbia.

Vick, S. G. (1983). *Planning, design, and analysis of tailings dams.* John Wiley & Sons Inc.

Walder, J. S., Iverson, R. M., Godt, J. W., Logan, M., & Solovitz, S. A. (2015). Overtopping of Noncohesive Earthen Dams. *Water Resources Research*, *51*, 6701–6724. https://doi.org/10.1002/2014WR016620.Received

West, M., Morris, M., & Hassan, M. (2018). *A guide to breach prediction*.

https://doi.org/10.1680/jdare.18.00031

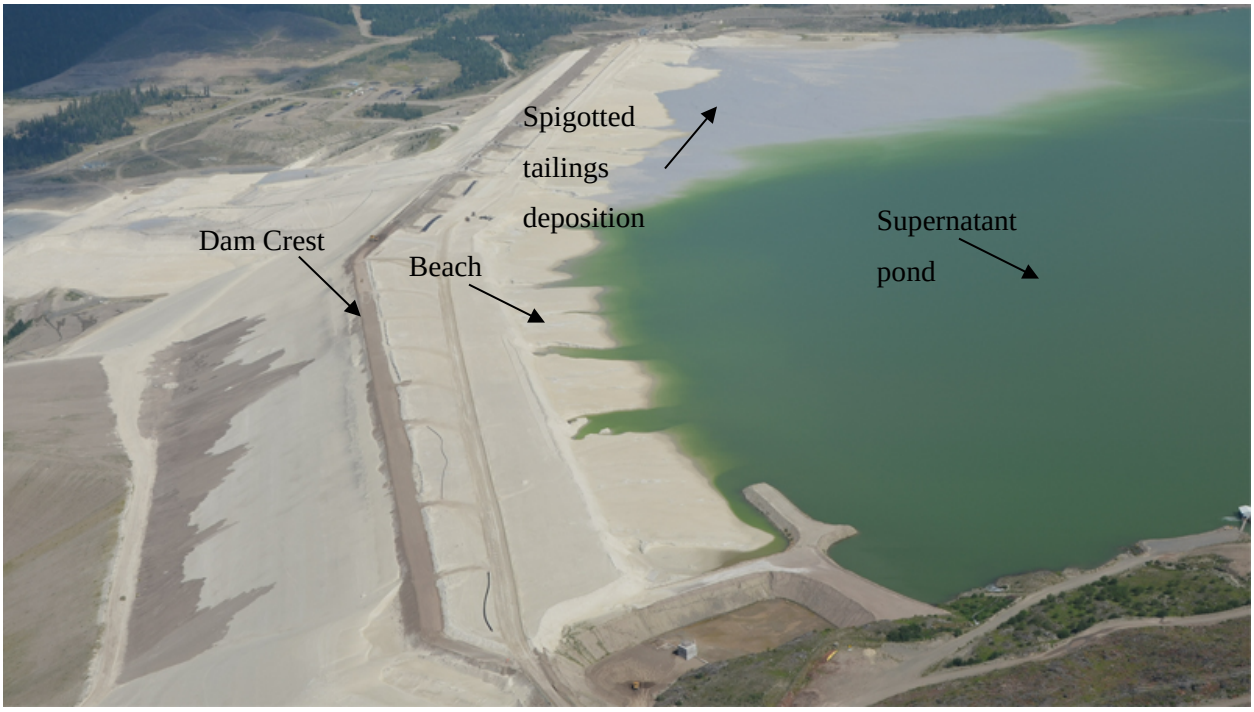

Figure 1.1: Tailings storage facility at Teck Resource Ltd.'s Highland Valley Copper mine. Note tailings beach that has formed upstream of dam crest and tailings slurry deposition (Teck.com)

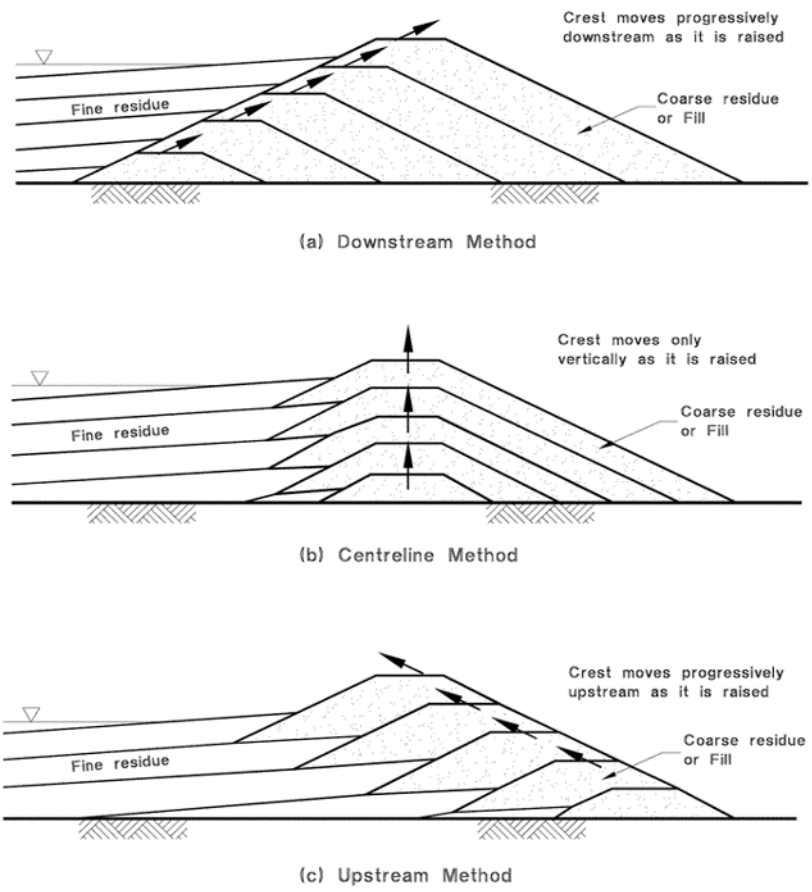

Figure 1.2: Tailings dam design methods (Vick, 1983)

Figure 1.3: 2015 Samarco tailings dam breach (Estãdo.com)

Figure 1.4: USGS dam breach test facility in the H.J. Andrews Experimental Forest (Walder et al., 2015)

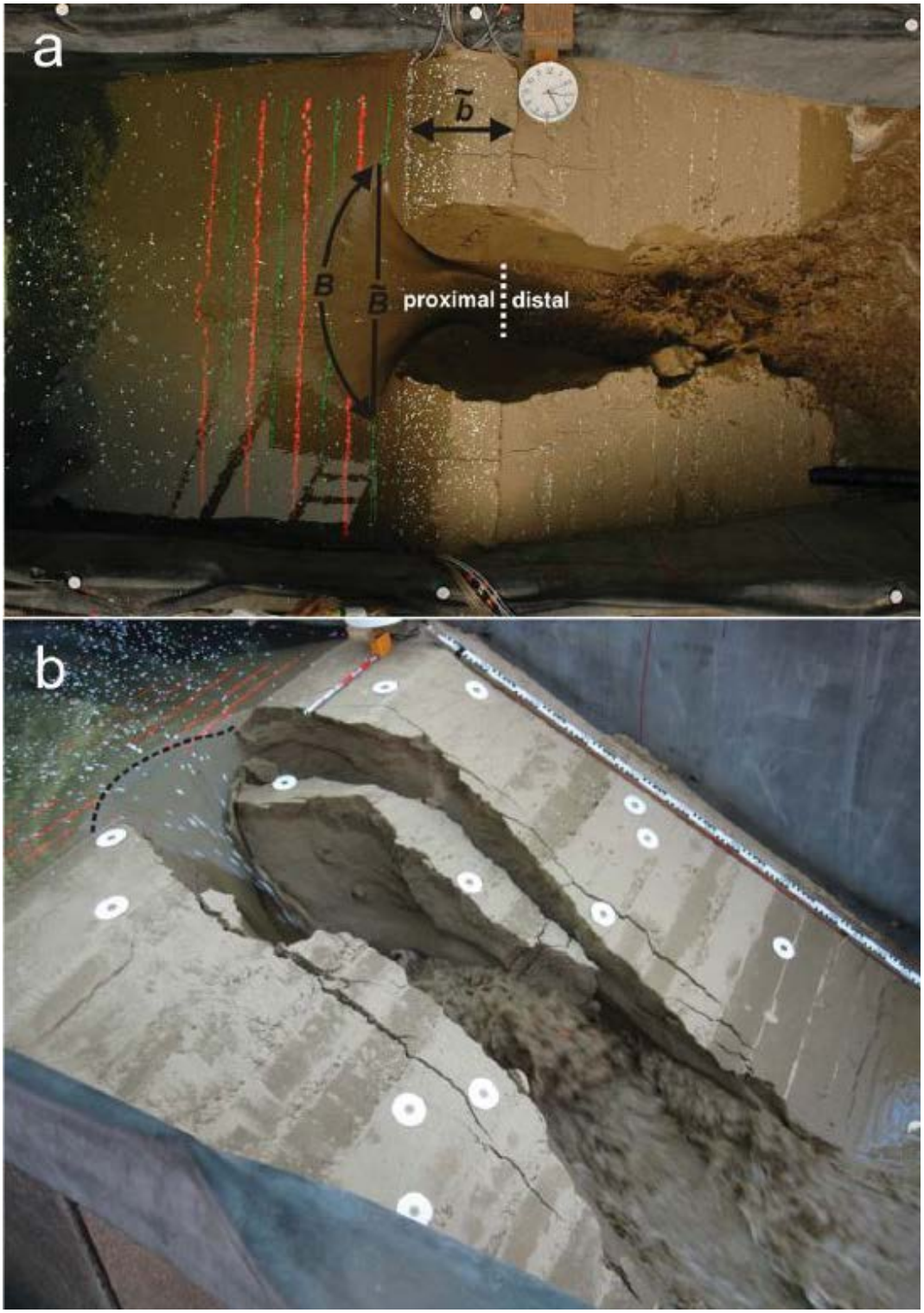

Figure 1.5: Breach crest geometry, observed during failure (Walder et al., 2015)

Chapter 2

Effect of reservoir and upstream dam geometry on peak discharge during overtopping breach in noncohesive homogenous embankment dams

2.1 Introduction

Dam breach is failure of a dam structure resulting in the uncontrolled release of retained materials in a sudden or catastrophic manner (Martin et al., 2015). Tailings dams exhibit an alarmingly high frequency of catastrophic failure, with recent notable examples including the 2014 Mount Polly dam in British Columbia, Canada, the 2015 Fundão dam breach in Minas Gerais, Brazil, the slumping failure in 2018 at Cadia mine in New South Wales, Australia, and the 2019 disastrous rapid release of retained materials at Córrego do Feijao in Brumadinho, Brazil. Failure at this high rate of occurrence and level of consequence would not be tolerated in general engineering practice (Saiyar et al., 2019), yet over the past century, almost 3,000 lives have been lost as a result of breach of tailings dams (Santamarina et al., 2019). Action is urgently needed to modify tailing dam designs and engineering practice to lower the probability of failure and to better manage the risk associated with dam breach. The focus of this paper is the latter; specifically, to increase our understanding of dam breach processes to improve dam breach analyses relevant for the specific case of tailings dams.

Dam breach analyses are conducted to limit hazard exposure and potential for loss of life imposed by dams by informing dam hazard rating, flood-routing analyses, land use planning, flood mitigation strategies, and emergency response plans (e.g. CDA, 2007). The key relationship at the core of these efforts is the prediction of the outflow hydrograph, which is defined as the time rate of outflow during the breach event (West et al., 2018). Models developed to predict the outflow

hydrograph for water-retaining dams are generally divided in the literature into two classes: parametric and physically-based. Parametric models rely on regression analysis of empirical breach behaviour in historical failures to describe breach parameters as a function of dam or reservoir properties. In contrast, physically based models use fundamental principles of hydraulics, sediment transport, and soil mechanics to predict breach behaviour (Wahl, 2017). A comprehensive review of existing breach models by West et al. (2018) indicate that physically based models are generally more accurate and reliable than parametric models, although parametric models require less computing time and are commonly used in practice.

Flume and field experiments have played a central role in improving our understanding of dam breach processes and the development of physically based models. Notable studies include key contributions from the University of Auckland (Coleman et al., 2002), the IMPACT project (Morris et al., 2007), the United States Department of Agriculture – Agricultural Research Service (USDA-ARS) research program (Hanson et al., 2005), and United States Geological Survey (USGS) (Walder et al., 2015). A key observation from Coleman et al. (2002) and explored in further detail by Walder et al. (2015) is that the outflow due to overtopping is hydraulically controlled by the geometry of the breach crest that forms as an erosional feature in the upstream face of the dam. During a breach event, the breach crest is defined by connecting a series of high points along streamlines flowing over the breach channel in which flow is perpendicular to the breach crest at all points along its length (Coleman et al., 2002). This location acts as a broad crested weir that separates subcritical flow upstream from supercritical flow downstream. As the volumetric flow rate discharged over the breach crest is governed by the size and shape of the breach crest (Walder et al., 2015), a prediction of the evolution of the breach geometry is essential for the prediction of the outflow hydrograph.

In the literature, the shape of the breach crest is defined by the breach width distance defined along the crest of the dam, *B**, and the breach arc length, *B*. Due to the curved shape of the breach crest, *B** will be shorter than *B* (Coleman et al., 2002). Figure 2.1 illustrates the upstream slope of a dam experiencing dam breach featuring the erosional breach crest feature formed in the upstream face of the dam and the parameters defining the instantaneous breach geometry. The depth of water flowing over the breach, *d*, varies in height from zero at the intersection of the breach crest with the reservoir water elevation to its maximum point at the arc apex.

Tailings dams differ from conventional water-retaining dams in design (e.g. upstream, central, downstream construction), materials retained behind the dam and used in construction of the dam, and of particular importance to breach analyses, the inclination of the upstream face of the dam. To reduce the risk of seepage induced failure (i.e. piping), shallowly sloping tailings beaches are often constructed from fine grained tailings material to reduce the hydraulic gradient and the quantity of seepage flow at the dam face (Mcleod & Murray, 2003). The typical upstream geometry of a tailings dam therefore is inclined much shallower than would be constructed for a water retaining dam. Given that the shape of the breach crest in the upstream dam face has been observed to quantitatively define the outflow hydrograph (e.g. Walder et al., 2015), it is reasonable to hypothesize that the outflow hydrograph for the shallowly inclined upstream dam face associated with tailings dam geometry will differ from that of a clear water dam. However, models currently used in breach studies of tailings dams have been adapted from those developed for more steeply sloping water storage dams, and have not yet been validated for the tailings case. It is currently unclear whether this is a conservative approach for estimating tailings dam breach outflow, and if so, to what degree.

The objective of this study is to use detailed observations of breach initiated by overtopping in six large physical model dams of varying upstream slope angles ranging from steep (e.g. clear water dams) to shallow (e.g. tailings case) to define, for the first time, the effect of the upstream slope angle on the breach outflow hydrograph. In the remainder of this chapter we describe the experimental program, and instrumentation including a specific strategy to capture the evolution of the geometry of the upstream breach crest. Based on these observations, we then introduce a mathematical framework to quantify the instantaneous geometry of the breach using a simplifying assumption of a semi-elliptical shape of the breach crest. We then illustrate how this framework can be paired with a discharge equation to generate quantitative estimates of peak breach outflow for differing upstream slope angles including those relevant to the calculation of the breach outflow hydrograph for the shallowly sloping upstream slope angles associated with tailings dams.

2.2 Experimental Methods and Materials

2.2.1 Experimental Program

A test series comprising of six large physical model dams (1 m high) was designed to investigate the effect of upstream slope angles ranging from 10.0° to 30.0° from horizontal on the outflow hydrograph generated during dam breach by overtopping. All dams were constructed with a downstream slope inclination of 3H:1V or 18.4° (Figure 2.2a). Details of the test matrix are presented in Table 2.1, including the context of the configuration previously investigated by Walder et al. (2015) and Coleman et al. (2002). To enable as direct a comparison with the work of Walder et al. (2015) as practically possible, the geometry of the dam physical models adopted in the present study used the same dam height (1.0 m), a nominally identical dam width (2.09 m) and crest breadth (0.3 m), and for the base case, an identical upstream slope angle (30.0°). Notable differences between these studies include the downstream slope angle (18.4° vs 30.0° by USGS), a different reservoir stage-volume relationship (discussed later in the manuscript), and tailwater submergence

in the present study. Based on the conclusions of Walder et al., 2015 that discharge is controlled by the breach crest located upstream of the dam crest, differences in downstream geometry and tailwater submergence of the downstream toe were considered to be of little consequence to test results. The shallower downstream geometry was selected as a practical choice in terms of constructability and in light of this study's focus on tailings facilities, where a 30.0° downstream slope angle would generally be considered quite steep.

As shown in Figure 2.2b, the physical model dams of the present study were constructed in the 36 m long horizontal portion of the Queen's University Landslide Flume (e.g. Bullard et al., 2019; Mulligan et al., 2019). The crest of the dam was positioned at the approximate mid-point of the horizontal portion of the flume, to permit roughly equally sized upstream reservoir and downstream deposition zones. In other words, the experiment was designed to permit an upstream reservoir to overtop the dam at an elevation of approximately 1 m, and to enable the observation of breach flows leading up to the peak outflow before the upstream and submerged downstream water levels reach equilibrium at an approximate reservoir elevation of 0.5 m. As the work of Walder et al. (2015) indicates that the outflow hydrograph is hydraulically controlled solely by the upstream geometry of the breach crest, it is hypothesized that the tailwater submergence in the present study will not impact the outflow hydrograph. The validity of this hypothesis will be revisited later in the manuscript.

2.2.2 Materials and construction methods

Dams constructed in this study present a first order approximation for experimental purposes and do not reflect conventional heterogenous construction employed in a prototypical setting. Each dam was constructed from uniform fine sand (#730 Silica Sand by Weldon Company) that possesses a grain size distribution nominally identical to F110 Ottawa sand with a mean grain size, d_{50}, of 0.12

mm. The uniform fine sand utilized by Walder et al. (2015) had a larger d_{50} of 0.21 mm, however, both sands are described as “fine sand” by the Wentworth grade chart, and were considered to be reasonably similar. Comparison of laboratory data by Walder et al. (2015) to Coleman et al. (2002), which included model dams constructed of uniform noncohesive material with d_{50} ranging between 0.5 mm to 2.4 mm, demonstrated a small increase in peak discharge with d_{50}. Review of several further studies by Walder et al. (2015) regarding the effect of grain size on peak discharge revealed conflicting observations and concluded that if any relation does exist, it could be considered a second order effect. Therefore, the grain size of the sand utilized in this study was considered to have little effect on peak discharge results and results can largely be considered comparable to those of Walder et al. (2015) and Coleman et al. (2002).

Triaxial tests conducted on the #730 fine sand indicate that the constant volume angle of internal friction of the material is 30.5° (Beddoe & Take, 2016), defining the upper bound of upstream slope angles possible to be tested in the study.

The construction process for each dam is illustrated in Figure 2.3. The base of the concrete flume prior to dam construction is illustrated in Figure 2.3a. The most prominent feature in the photograph is the presence of the 10.2 cm diameter toe drain constructed from two sections of corrugated high density polyethylene (HDPE) drainage pipe that was installed under the dam crest, flush to the flume base and secured to the floor with metal strapping. A perforated 2.0 m long pipe section was located parallel to the crest and wrapped in geotextile fabric to allow for water ingress while providing a barrier to the sand material. The perforated pipe section was attached to a solid (non-perforated) 3.5 m long pipe section with an L-joint, extending from the dam crest to beyond the downstream toe of the dam. The outline of the downstream face of the dam was defined using aluminum angle brackets anchored to the concrete sidewalls of the flume.

Sand was deposited into the flume with a Bobcat skid steer loader (Figure 2.3b) for later placement. The construction methods of the dams included a variety of techniques including hydraulic placement, shovelling and hand tamping (Figure 2.3c). Hydraulic placement was a method that allowed for relatively consistent construction across tests, while not requiring the sand to be dried to an optimal moisture content following each test or utilization of traditional compaction techniques (e.g. construction in lifts, vibratory compaction). Density was measured prior to reservoir impoundment with a nuclear density gauge at three points on the dam crest and one point on the downstream slope 1 m from dam crest, prior to each test, and is reported in Appendix A. Generally, density measurements were similar across all tests, however some variation in downstream water content was noted. Dams were deliberately constructed in a "as loose as possible" state to investigate liquification susceptibility. The average measured dry density of the dam material, 1517 kg/m^3, was similar to the dry density reported by Walder et al. (2015) of 1514 kg/m^3.

In order to contain the sand in the desired dam geometry, formwork was constructed from plywood sheets. The plywood sheets were saw-cut to allow for drainage, then wrapped in geotextile fabric to hold the sand in place. Aluminum angle brackets were drilled into the flume side walls, inclined at 18.4° from horizontal on each of the downstream sidewalls and inclined at angles ranging from 10.0° to 30.0° from horizontal on each of the upstream sidewalls. The plywood formwork was then sequentially bolted to the brackets as sand was deposited (Figure 2.3d). Sand was liquefied into slurry form for hydraulic placement by jetting the sand with high pressure water. Generally, the slurry sand:water ratio was 1:3 based on bottle samples taken during pumping. The slurry was pumped into place with a Tsurumi HSD 2.55S submersible single-phase portable slurry pump, and a 186 W submersible puddle pump was utilized with the form work area to quickly evacuate ponded water.

Following construction, dams were left to drain for several days prior to removing the formwork. After the formwork was removed, any additional sand required to form the desired shape was shovelled into place, hand tamped and smoothed with a trowel (Figure 2.3e).

After each breach test, several days were allowed for drainage of the flume and deposited sand material. Finally, the sand in the downstream area was moved back upstream for construction of the next dam by shovelling and with a Bobcat 325 excavator.

2.2.3 Instrumentation

The test instrumentation was specifically designed to capture the instantaneous breach crest geometry. The falling height of water in the reservoir during the test results in a variable scale factor between linear distances and pixels due to refraction. Scales were marked on aluminum angle brackets drilled into the flume side walls, allowing for calculation of a scale factor for each image analyzed that accounted for the differences in refraction as the reservoir water level decreased.

The dam structure was homogenous, constructed entirely from the same light coloured material. To provide increased contrast for image analysis, a thin layer of sand dyed black with India ink was placed on the surface of upstream dam slope. The breach crest shape could then be more clearly and consistently delineated from discrete images, where it was measured as the shape along the boundary between the dark sand (uneroded) and light sand (eroded).

The breach crest evolution was measured on plan view images captured by four Canon EOS Rebel T5 cameras Digital Single-Lens Reflex (DSLR) with 18-55 mm focal length lenses, mounted to a rotating support beam. The beam was constructed to suspend cameras above the dam, along the

flume centreline. When in its upright position, cameras mounted to the beam were located 2.5 m above the dam crest elevation, capturing a combined field of view of approximately 8.0 m in length. This structure pivoted about two bolted connections, allowing for access to cameras between tests (Figure 2.3f). The cameras each had an 18 megapixel APS-C 22.3 mm by 14.9 mm sensor. The cameras were synchronized and images were acquired every five seconds during breach with a synchronized remote intervalometer.

Qualitative video was captured throughout each test with a Canon EOS Rebel T5 camera positioned downstream of the dam, oblique to the downstream face. Plan view video was recorded with a GoPro Hero 3 camera, also attached to the rotating support beam. Additional plan view video was recorded with a Canon EOS Rebel T5 camera, mounted to a tall extendable tripod, located against the exterior wall of the flume, near the dam crest.

Reservoir elevation was monitored with five Akamina AWP-24 wave capacitance height gauges, distributed longitudinally upstream of the dam along the reservoir centreline, set to a sampling frequency of 100 Hz. Discharge over the dam during breach was calculated from the change in reservoir elevation over the known reservoir geometry. One wave height capacitance gauge was also positioned 1.0 m downstream of the dam toe to monitor outflow downstream of the dam.

2.2.4 Test procedure

Upon completion of dam construction, cameras attached to the rotating camera mount were connected to AC power, the mount was raised into position over the dam, and secured with guy lines. A pre-failure laser scan of each dam was completed with a Faro Laser Scanner Focus^{s} 150, with three scanning locations required to capture the upstream, downstream and crest of the dam

due to occlusions. Additional laser scans were completed of the downstream deposit and remaining dam structure following failure.

To initiate failure by overtopping, a v-notch approximately 6 cm wide by 6 cm deep with side slopes of 45° was incised into the centre of the dam crest with a piece of aluminum angle bracket prior to filling the flume reservoir. This notch size was sufficiently small to encourage a slow initiation phase of breach, whereas a substantially larger initial notch would have resulted in short initial phase. As the reservoir was filled, calibration of the capacitance wave height gauges was conducted. When water entered the v-notch, the water tap was turned off. As the first bead of water flowed through the notch and reached the downstream toe of the dam, data acquisition with the capacitance wave height gauges and plan view cameras was started simultaneously. The qualitative cameras began recording slightly after this time.

During several tests, sediment grab samples were taken downstream of the dam, around the time of peak discharge. The sand and water volumes of each sample were measured in a graduated cylinder and recorded.

2.3 Observations of Dam Breach

2.3.1 Breach evolution

The breach process for noncohesive earthen embankments, where overtopping is initiated with a v-notch incision in the crest, can be described by three sequential stages, previously detailed by others including Visser et al. (1995), Coleman et al. (2002), and Walder et al. (2015). Photos of the breach evolution, observed from a downstream oblique view are presented in Figure 2.4.

In Stage 1, the v-notch slowly begins to increase in size, however, since the downstream face of the dam is not fully saturated, some of the water and sediment exiting the notch infiltrates and is deposited on the downstream dam face, respectively. Eventually, as the downstream face of the dam in the vicinity of this infiltration becomes saturated, the notch outflow incises a narrow channel into the downstream face. The stage ends when the incised channel reaches the downstream toe (Figure 2.4 a,b).

In Stage 2, the incised channel begins to form steps beginning at the toe of the dam, retrogressing toward the crest. The channel is widened by slumping blocks of undercut material, usually alternating from one side of the channel to the other. The stage ends when the stepping channel intersects with the breach crest (Figure 2.4 c,d).

In Stage 3, the final stage, discharge increases rapidly, as a path between the stored volume in the reservoir and downstream dam toe has been opened. The breach channel widens quickly as increasing outflow continues to undercut the channel banks, and the channel is eroded both laterally and vertically. Peak discharge is reached, and as the outflow is decreasing, the channel continues to erode until the end of the breach. The end of the stage coincides with the end of breach process (Figure 2.4 e-h).

Walder et al. (2015) conducted six breach tests to demonstrate the reproducibility of the outflow hydrograph. Each dam in this test series was constructed using the same methods and maintained a constant geometry. They showed that by selecting the time datum, T=0, as the onset of Stage 3, the time of rapid increase in outflow, test to test variations in outflow hydrographs were small and behaviour could be directly compared. This approach has also been applied to the outflow hydrographs presented in this study, as it was previously demonstrated to account for variability in

the saturation of dam downstream face, reflected in morphological Stage 1 and 2, which was not tightly controlled in this study.

2.3.2 Outflow hydrographs

Discharge with time throughout the breach process was calculated utilizing reservoir elevation data captured by upstream wave capacitance gauges, and the reservoir geometry. Peak discharge was observed to increase as the upstream slope angle increases, ranging from 0.07 m^3/s for a 10.0° upstream slope to 0.24 m^3/s for a 30.0° upstream slope (Figure 2.5a). It can also be seen that there is reasonably good repeatability for the tests with 18.4° and 30.0° upstream slope angles, and that time to reach the peak discharge value decreases as slope angle increases, ranging from 120 seconds for a 10.0° upstream slope to 75 seconds for 30.0° upstream slope. In the case of Test S2, peak discharge was taken at the time the discharge rate slowed significantly, though this was not the absolute maximum value observed.

Due to the small drain in the depositional zone, the maximum reservoir elevation decrease during breach was limited by the size of the flume downstream of the dam. The equilibrium water level, between the dam reservoir and depositional area, was a function of the upstream geometry of the dam, as the downstream geometry was constant for all tests (Figure 2.5b).

A linear relationship between peak discharge and the dam upstream slope angle was identified (Figure 2.5c). However, this linear relationship does not describe the peak discharge observed by Walder et al. (2015), for the same upstream dam geometry. Therefore, upstream slope angle alone cannot fully describe peak discharge. This is an interesting observation that will be further explored later in this paper in Section 2.3.7.

2.3.3 Breach geometry

Breach geometry throughout failure was measured on the plan view images captured at five second intervals during breach. Figure 2.6a shows the breach evolution captured during a typical test, in this case with an upstream slope angle of 30.0°. The breach crest was manually identified in the images. The surficial black sand layer placed on the upstream dam face provided contrast between the upstream face (black) and eroded breach crest (white). On the images, this boundary has been identified in red. The shape of the breach was observed to be more rounded for the dam with an upstream slope of 10.0° (Figure 2.6b). This results in the breach arc length, B, being longer in comparison to other tests.

B* and B were measured for a select number of images during failure, between time T=0 (start of Stage 3) and the point where the breach shape was observed to be limited by the flume side walls. (Figure 2.7a and Figure 2.7b, respectively). For the period of the breach process where data was collected, the breach width and arc length growth rate can be broadly described as linear with respect to time.

The ratio of B/B* is presented in Figure 2.7c. The results observed at the Queen's University laboratory were within the range reported by Al-Riffai (2014) and Walder et al. (2015) of 1.05 to 1.45, with the exception of the dam with an upstream slope of 10.0°, which exceeded this threshold. This observation is consistent with the rounder shape and comparatively longer breach crest length for this test, noted above.

2.3.4 Ellipticity index

Review of the plan view images shows that the breach shape generally resembles a semi-ellipse. Taylor et al. (2018) observed that shape of landslides is generally elliptical and quantified the

degree of ellipticity of the landslide with an ellipticity index. The ellipticity index, a measure of how well the observed shape fits to the geometric definition of an ellipse, has been adapted here to measure the degree of semi-ellipticity of the breach crest:

$$e_B = 1 - 2\frac{A_B - A_{B\cap E}}{A_B} \qquad (1)$$

where:

e_B = breach semi-ellipticity index

A_B = original breach area

$A_{B\cap E}$ = area of geometrical intersection between original breach shape and its idealized elliptical shape

A perfect fit would be where the area of the breach exactly overlaps with the area of an ellipse, $A_B = A_{B\cap E}$, so $e_B = 1$. The degree of semi-ellipticity of the dam breach is generally greater than 0.9, so a semi-ellipse shape can describe the shape of the dam breach crest very well (Figure 2.8a).The breach shape throughout failure was shown to maintain this semi-elliptical shape when the calculated semi-elliptical shape is plotted against the measured shape extracted from the plan view images (Figure 2.8b).

2.3.5 Breach ellipse parameters

As described above, the breach shape can be well described by a semi-ellipse. Based on the method by Ramanujan (1914), the perimeter of the semi-ellipse (breach crest arc length) is approximately equal to:

$$B \approx \frac{\pi\left[3(a+b) - \sqrt{(3a+b)(a+3b)}\right]}{2} \qquad (2)$$

The ellipse shape is typically described by its major axis, a and minor axis, b. If a semi-ellipse is fit to the breach shape, the major axis a, aligns with the breach width, B*, where a=B*/2.

From geometry, the depth flowing over the breach crest can then be determined at any point along the crest by:

$$d = x * tan\alpha \qquad (3)$$

where:

d = depth over breach (m)

x = perpendicular distance from point of water surface intersection with upstream dam face to breach crest (m)

α = dam upstream slope (°)

The ellipse minor axis b, measures the maximum perpendicular distance from the intersection of the breach crest with the reservoir water elevation, to the intersection with the breach crest (Figure 2.9).

As shown in Figure 2.10a and Figure 2.10b, calculations of the ellipse parameters a and b, respectively, produce largely linear trends, which is to be expected as they are a function of B*, which was shown earlier to increase linearly with time. Similarly, the average depth flowing over the breach crest throughout the breach event, calculated with Equation (3), presents a linear trend (Figure 2.10c).

The aspect ratio, a/b, describes the proportional relationship between the major and minor axes of the ellipse (Figure 2.10d). The mean value of a/b was 1.43 ± 0.28, ranging from about 0.9 to 2.2 across all tests. Though a/b was variable throughout the failure, it was observed to be somewhat constant between 20 seconds to 80 seconds in all tests. Data acquisition during breach was limited to about 100 seconds, or before the breach crest began to be limited by the flume width. The

relatively constant a/b ratio during the monitored period of the breach event indicates that as the breach crest grew larger, the elliptically shaped breach crest grew proportionately along both axes.

2.3.6 Rating Curve

In hydraulics, a rating curve communicates the integrated effect of stream geometry and hydraulic parameters, converting flow height to volume (Chubak & Mcginn, 2002).

The discharge equation to describe flow over the breach crest employed by Walder et al. (2015) was:

$$Q = C_d \left(\frac{2}{3}\right)^{3/2} g^{1/2} B < E >^{3/2} \qquad (4)$$

where:

Q = discharge (m^3/s)

C_d = discharge coefficient (dimensionless)

g = acceleration due to gravity (m/s^2)

B = breach crest arc length (m)

<E> = mean specific energy (m)

At an average depth along the breach crest, d_{avg}, <E> can be written as:

$$< E > = \frac{v^2}{2g} + d_{avg} \qquad (5)$$

where:

v = mean flow velocity (m/s)

d_{avg} = average depth flowing over breach crest (m)

The Froude number is a hydraulic relationship of the ratio of gravitational forces to inertial forces, and provides a method of classifying flow conditions, defined as:

$$Fr = \frac{v}{\sqrt{g * d_{avg}}} \qquad (6)$$

where:

Fr = Froude number (dimensionless) (Yalin & Da Silva, 2001)

The breach crest has previously been described as the location of critical flow, separating upstream subcritical flow and downstream supercritical flow. However, as discussed by Walder et al. (2015), due to the strong curvature of the streamlines at the breach crest, relationships for steady, uniform, rectangular flow cannot be applied to the elliptically shaped weir, specifically, the critical Froude number does not equal 1 at this location (Castro-Orgaz & Chanson, 2009). Walder et al. (2015) calculated the critical Froude number at the breach crest to be 0.74 ±0.14 utilizing laboratory data. In other words, the Froude number will equal 1 slightly downstream of the breach crest location.

The flow velocity was not measured during this experiment as any technique available at the time of testing would have obscured images required for breach geometry analysis. Therefore, a Froude number at the breach crest of Fr=0.74 was adopted based on the work by Walder et al., 2015, due to comparable dam dimensions and materials. Fr=0.74 can be substituted into Equation (5) to solve for the average flow velocity, and Equation (6) can be re-written as:

$$< E >= 1.274 d_{avg} \qquad (7)$$

If a Froude number of Fr=1 was utilized in analysis, this would have resulted in a 13.5% reduction in calculated mean specific energy at the breach crest.

A rating curve has been developed for this test series, comparing measured outflow to the outflow calculated utilizing Equation (4), without a discharge coefficient value (Figure 2.11). This plot also includes data presented by Walder et al. (2015). The slope of the rating curve is equal to the discharge coefficient, C_d. C_d can be thought of as a correction factor, which accounts for observed differences between discharge measured in the laboratory and the theoretical discharge calculated with the discharge equation. The C_d value for this test series was found to be 0.98, which is close to that reported by Walder et al. (2015) of C_d=0.96. Two tests conducted at Queen's have been omitted from the C_d calculation due to the reservoir being filled for a long period of time pre-test, possibly resulting in over calculation of depth flowing over the breach crest due to variation in post impoundment geometry from the design geometry (e.g. wetting collapse). The rating curve suggests that the outflow equation presented by Walder et al. (2015) is a good method to describe outflow over the breach crest for an elliptically shaped breach crest.

2.3.7 Peak Outflow Calculation

As discussed in Section 2.3.2, the dam upstream slope angle alone could not describe peak outflow for dams with equal upstream geometries constructed in both the reservoir at Queen's University and the reservoir constructed by Walder et al. (2015). However, the shape of the reservoir storage function for the two facilities was different, and the total volume available for release during breach was about 13 m^3 at the USGS facility, compared to roughly 16 m^3 at the Queen's facility (Figure 2.12). As will be detailed below, the available reservoir volume is critical in determination of peak discharge.

From the elliptical breach geometry definition, it has been established that the depth of water over the breach at the intersection of the breach crest with the reservoir water elevation is zero, or in

other words, the depth of water in the reservoir, H, is equal to the dam height, D. At every other point along the breach crest, the depth of water in the reservoir must be equal to the depth flowing over the breach crest plus the dam height (H=d+D). If the reservoir elevation becomes less than this condition (H < d+D), the discharge rate is limited, as the reservoir is unable to completely fill the available breach crest area. Discharge will decrease due to a decreased depth flowing over the breach. Peak discharge has been reached when this reservoir elevation condition can no longer be satisfied (Figure 2.13).

To calculate breach outflow based on the discharge equation, the breach crest geometry was defined based on laboratory data. A general breach width growth rate, based on a linear regression of B* vs time, is shown on Figure 2.7a.

Since the breach crest was found to be elliptical, the ellipse aspect ratio can be used to calculate the breach crest arc length, B, based on the horizontal breach crest width, B*, and the aspect ratio, a/b. The mean aspect ratio, a/b=1.43 has been used in this analysis. Next, the depth flowing over the breach crest can be calculated based on the upstream slope angle. Finally, incremental discharge can be calculated with the discharge equation and C_d=0.98 from the rating curve in Figure 2.11. To calculate peak discharge, this iterative calculation is repeated until condition H<d+D is true.

In contrast to the peak discharge relationship based on upstream slope angle alone, the method described above can be used to accurately calculate the peak discharge rate and time to peak for dams with upstream slope angles of 30.0° in each of Queen's University and USGS reservoirs (Figure 2.14a). Further, this method is also applicable for dams with upstream slope angles ranging from 10.0° to 30.0°, with a constant reservoir, exemplified by the calculation of peak discharge

compared to measured peak discharge for each dam in this test series constructed in the Queen's University flume (Figure 2.14b).

Post-peak discharge behaviour has not been calculated in this study due to the limitation of the flume width. Generally, breach behaviour transitioned from 3D to 2D soon after peak discharge was reached, and data collection stopped. As such, the 3D breach crest width growth rate behaviour post-peak discharge is unknown.

2.4 Conclusions

A key finding of this study is that a semi-ellipse can describe the shape of an upstream hydraulic control section breach crest. It is this upstream feature, at the location of critical flow, which governs breach discharge, and not the chaotic slope failure and erosion events occurring in the breach channel downstream. Further, the profile of water flowing over the breach crest is also semi-elliptical shaped, with water depth increasing from zero at the intersection of the breach crest with the reservoir water elevation, to its maximum point below the apex of the breach crest semi-ellipse.

The growth rate of the breach crest horizontal length, B*, and breach crest arc length, B, was found to increase linearly with time from the time datum, at the onset of morphological Stage 3, to the point where the experiment transitioned from a 3D to 2D scenario (flume width limit reached). This transition coincidently occurred around the time peak discharge was reached for most tests in this study. Within the geometric framework of a semi-ellipse, the shape aspect ratio, a/b, was calculated. It was observed to be reasonably steady between time T=20 to T=80, or the majority of the period where data was collected. By combining a constant ellipse aspect ratio with a linear breach crest growth rate, the size and shape of the breach crest can be numerically calculated throughout failure.

Discharge over the breach crest was calculated using the same equation presented by Walder et al. (2015). The Froude number, Fr=0.74, observed at the breach crest in that study was assumed to be similar here. Discharge calculated based on data from this test series also fit reasonably well on the rating curve presented by Walder, indicating that their discharge equation can describe both experiments. Al-Riffai and Nistor (2011) showed that peak discharge was inversely correlated to peak discharge in terms of void ratio, and therefore the effect of density on peak discharge with respect to upstream slope angle warrants further research.

Finally, the influence of dam upstream geometry and the reservoir geometry was examined. It was observed early in the study that though there was a relationship between peak outflow and the dam upstream slope angle, this relationship was not valid for equally sized dams in differently shaped reservoirs. Peak discharge occurs at the point in the breach event when the breach crest is longest while the depth of water flowing over the breach is at its maximum. The breach discharge becomes limited by the reservoir capacity when the reservoir elevation, H, becomes less than the sum of the dam height, D, and the theoretical depth of flow over the breach crest, d. Given the dimensions of the dam and reservoir, a breach crest growth rate, and a semi-ellipse aspect ratio, discharge could be evaluated iteratively, reaching peak when this geometric condition was no longer satisfied. This methodology resulted in calculations of peak discharge and time to peak that were reasonably accurate for dams constructed in this study and selected dams from the Walder et al. (2015) study. Post-peak outflow calculations were not included due to the test flume width limitation, coincidentally restricting data collection after peak discharge was observed in most tests.

2.5 References

Al-Riffai, M. (2014). *Experimental Study of Breach Bechanics in Overtopped Noncohesive Earthen Embankments*. University of Ottawa.

Al-Riffai, M., & Nistor, I. (2011). Effects of compaction and slope steepness on the retreat of a sand bed under super-critical flow. *Proceedings of 34th IAHR Congress*. Brisbane, Australia.

Beddoe, R. A., & Take, W. A. (2016). Loss of slope support due to base liquefaction: Comparison of 1g and centrifuge landslide flume experiments. *Soils and Foundations*, *56*(2), 251–264. https://doi.org/10.1016/j.sandf.2016.02.008

Bullard, G. K., Mulligan, R. P., & Take, W. A. (2019). An Enhanced Framework to Quantify the Shape of Impulse Waves Using Asymmetry. *Journal of Geophysical Research: Oceans*, *124*(1), 652–666. https://doi.org/10.1029/2018JC014167

Castro-Orgaz, O., & Chanson, H. (2009). Bernoulli theorem, minimum specific energy, and water wave celerity in open-channel flow. *Journal of Irrigation and Drainage Engineering*, *135*(6), 773–778. https://doi.org/10.1061/(ASCE)IR.1943-4774.0000084

CDA. (2007). *Dam Safety Guidelines*.

Chubak, N. J. J., & Mcginn, R. A. (2002). A Rating Curve Based on Lake Levels: Evaluating Outlet flow for Clear Lake, Riding Mountain National Park, Manitoba. *Prairie Perspectives*, 18–31.

Coleman, S. E., Andrews, D. P., & Webby, M. G. (2002). Overtopping breaching of noncohesive homogeneous embankments. *Journal of Hydraulic Engineering*, *128*(9), 829–838. https://doi.org/10.1061/(ASCE)0733-9429(2002)128:9(829)

Hanson, G. J., Cook, K. R., & Hunt, S. L. (2005). Physical Modelling of Overtopping Erosion and Breach Formation of Cohesive Embankments. *Transactions of the ASCE*, *48*(5), 1783–1794.

Martin, V., Fontaine, D., & Cathcart, J. (2015). Challenges with conducting tailings dam breach studies. *Proceedings of Tailings and Mine Waste 2015 Conference*, 314–328.

Mcleod, H. N., & Murray, L. (2003). Tailings Dam Versus a Water Dam, What is the Design Difference? *ICOLD Symposium on Major Challenges in Tailings Dams*, 1–12.

Morris, M. W., Hassan, M. A. A. M., & Vaskinn, K. A. (2007). Breach formation: Field test and laboratory experiments. *Journal of Hydraulic Research*, *45*(SPEC. ISS.), 9–17. https://doi.org/10.1080/00221686.2007.9521828

Mulligan, R. P., Take, W. A., & Bullard, G. K. (2019). Non-hydrostatic modeling of waves generated by landslides with different mobility. *Journal of Marine Science and Engineering*, *7*(8). https://doi.org/10.3390/jmse7080266

Saiyar, M., Ryans, M., & Becker, D. E. (2019). Review of Recent Significant Tailings Dam Failures and Their Influence on Dam Safety Management. *Proceedings of 2019 CDA Annual Conference*. Calgary, Alberta.

Santamarina, J. C., Torres-Cruz, L. A., & Bachus, R. C. (2019). Why Coal Ash and Tailings Dam Disasters Occur. *Science Magazine*, *364*(6440), 526–528. https://doi.org/10.1126/science.aax1927

Taylor, F. E., Malamud, B. D., Witt, A., & Guzzetti, F. (2018). Landslide shape, ellipticity and length-to-width ratios. *Earth Surface Processes and Landforms*, *43*(15), 3164–3189. https://doi.org/10.1002/esp.4479

Visser, P. J., Kraak, A. W., Bakker, W. T., Smit, M. J., Snip, D. W., Steetzel, H. J., & van de Graaff, J. (1995). A Large-Scale Experiment on Breaching in Sand Dikes. *Proceedings of Coastal Dynamics '95*, 583–594. Gdansk, Poland.

Wahl, T. (2017). *Evaluation of Numerical Models for Simulating Embankment Dam Erosion and Breach Processes*. Denver, colorado.

Walder, J. S., Iverson, R. M., Godt, J. W., Logan, M., & Solovitz, S. A. (2015). Overtopping of

Noncohesive Earthen Dams. *Water Resources Research, 51*, 6701–6724. https://doi.org/10.1002/2014WR016620.Received

West, M., Morris, M., & Hassan, M. (2018). *A guide to breach prediction*. https://doi.org/10.1680/jdare.18.00031

Yalin, S., & Da Silva, A. M. F. (2001). *Fluvial Processes*. Delft, The Netherlands: International Associationof Hydraulic Engineering and Research.

Table 2.1: Slope Angle Sensitivity Test Series Details

Research Group	Test ID	Dam Height (m)	Crest Breadth (m)	Dam Width (m)	Upstream Slope (°)	Downstream Slope (°)	Pilot Notch Location	d_{50} (mm)	Q_{peak} (m^3/s)
Queen's University (present study)	S4	1.00	0.30	2.09	10.0	18.4	Flume Centre	0.12	0.07
	S1	1.00	0.30	2.09	18.4	18.4	Flume Centre	0.12	0.14
	S2	1.00	0.30	2.09	18.4	18.4	Flume Centre	0.12	0.16
	S5	1.00	0.30	2.09	25.0	18.4	Flume Centre	0.12	0.17
	S3	1.00	0.30	2.09	30.0	18.4	Flume Centre	0.12	0.24
	S6	1.00	0.30	2.09	30.0	18.4	Flume Centre	0.12	0.23
USGS (Walder et al., 2015)	1	1.00	0.36	2.00	30.0	30.0	Flume Centre	0.21	0.13
	2	1.00	0.36	2.00	30.0	30.0	Flume Centre	0.21	0.13
	3	1.00	0.36	2.00	30.0	30.0	Flume Centre	0.21	0.14
	4	1.00	0.36	2.00	30.0	30.0	Flume Centre	0.21	0.17
	5	1.02	0.33	2.00	30.0	30.0	Flume Centre	0.21	0.15
	10	1.00	0.36	2.00	30.0	30.0	Flume Centre	0.21	0.13
University of Auckland (Coleman et al., 2002)	N/A	0.30	0.07	2.21	20.3	20.3	Flume Sidewall	0.50	0.20

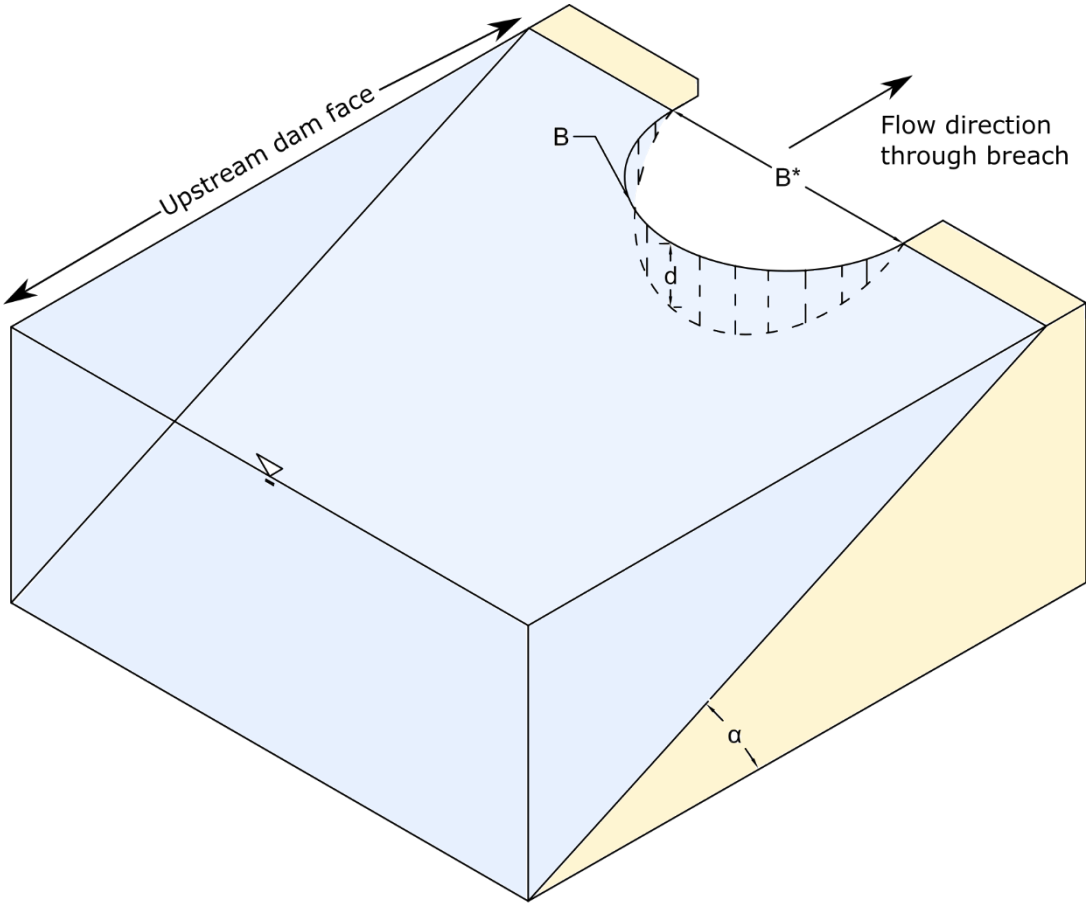

Figure 2.1: Schematic of dam breach geometry. B is the arc length distance of the breach crest, B* is the horizontal width between the two ends of the breach crest. The depth of water flowing over the breach, d, is geometrically related to the dam upstream slope angle, α.

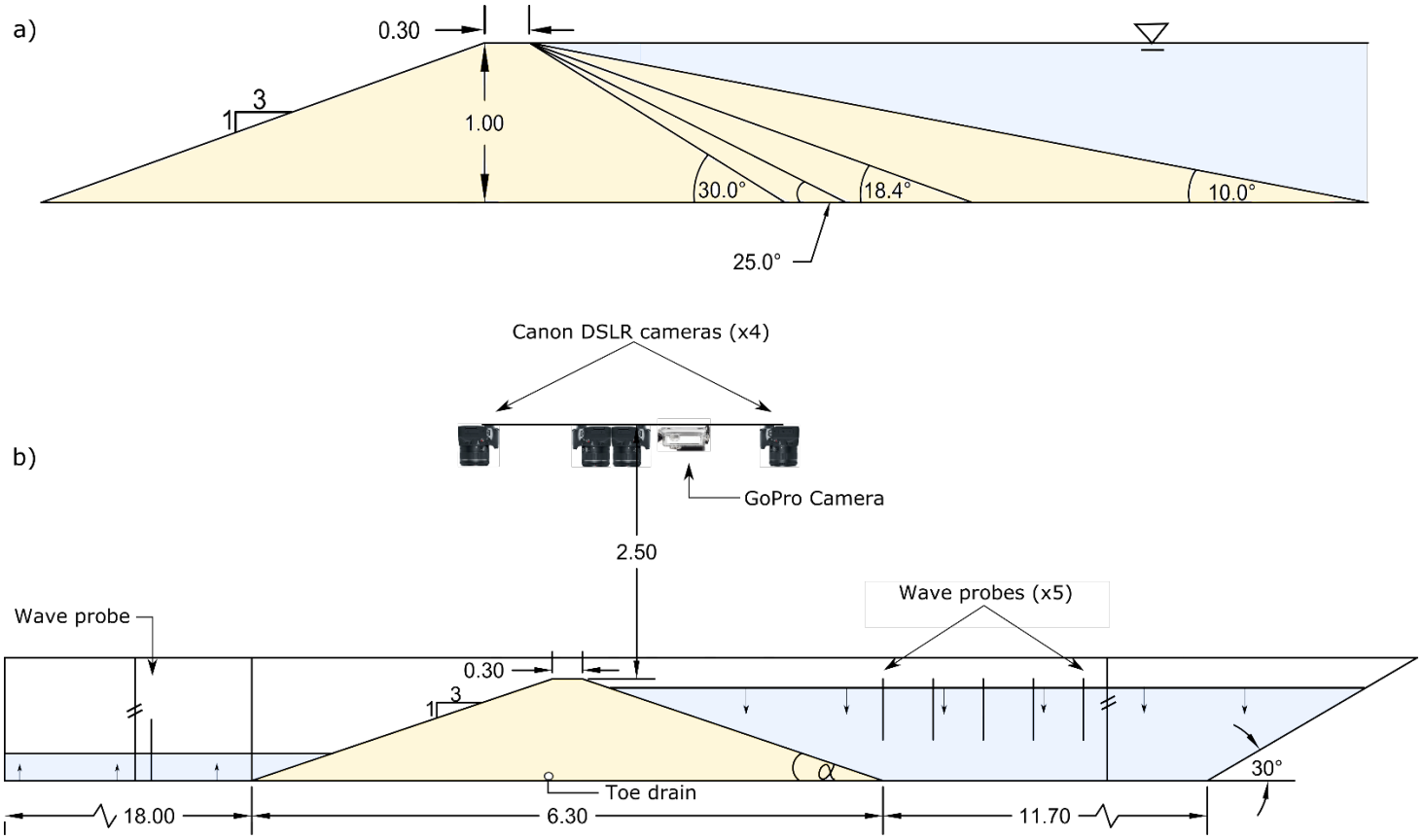

Figure 2.2: Test series experimental program. a) Dam upstream slope angle sensitivity– angles selected for testing b) Instrumentation setup The total horizontal flume length is 36 m, with the dam positioned approximately in the middle. The reservoir horizontal length is dependant on the dam upstream slope angle, *α*. In the schematic above, *α*=18.4°.

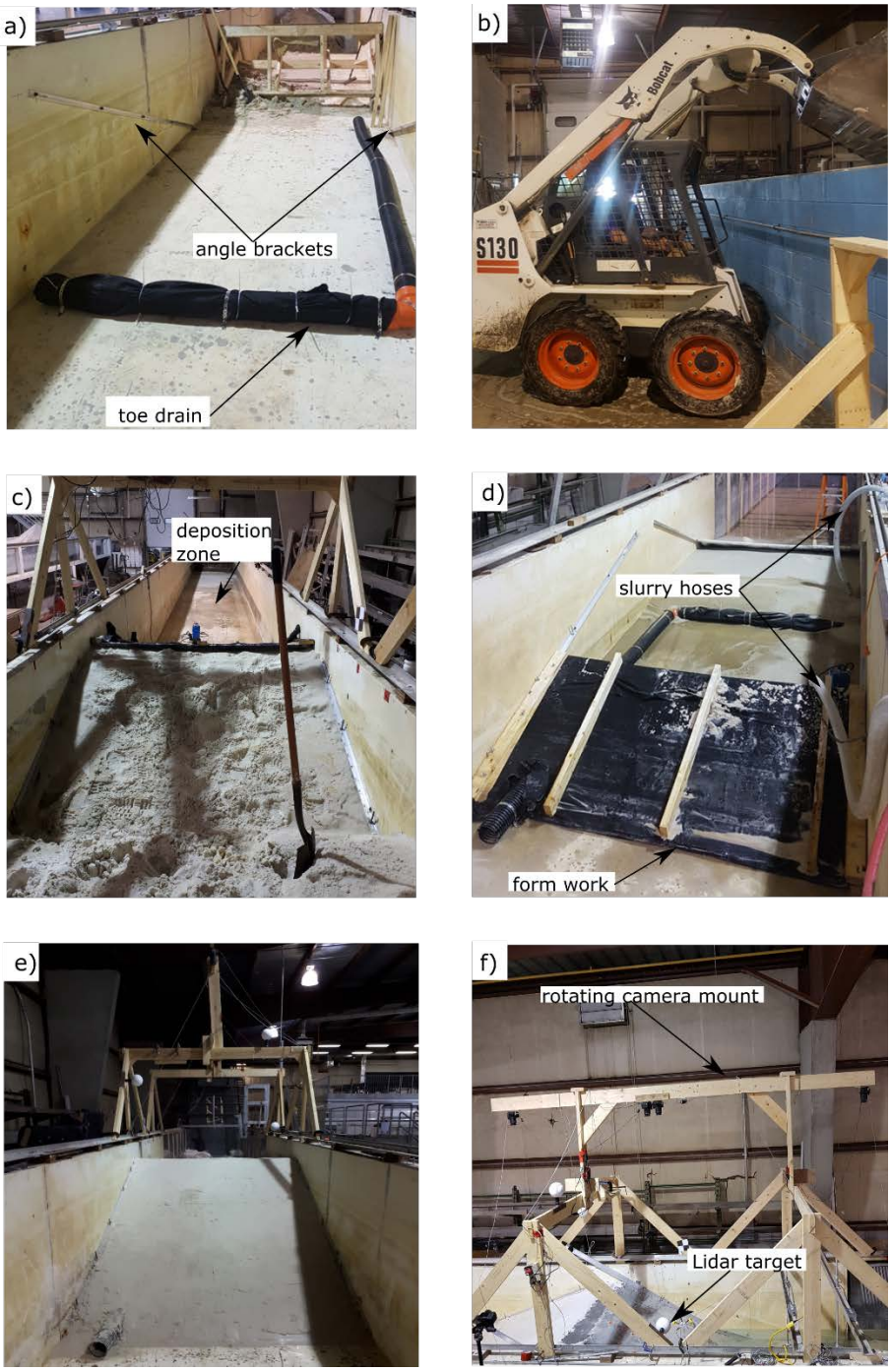

Figure 2.3: Images of the construction process. a) L-shaped toe drain drilled into the flume base prior to sand placement; b) Materials handling with Bobcat skid steer; c) Sand placement in progress; d) Slurry pumping sand between geotextile-wrapped plywood forms; e) Downstream view of finished dam, post surface smoothing; f) View of cameras mounted to the rotating support beam, in its upright position

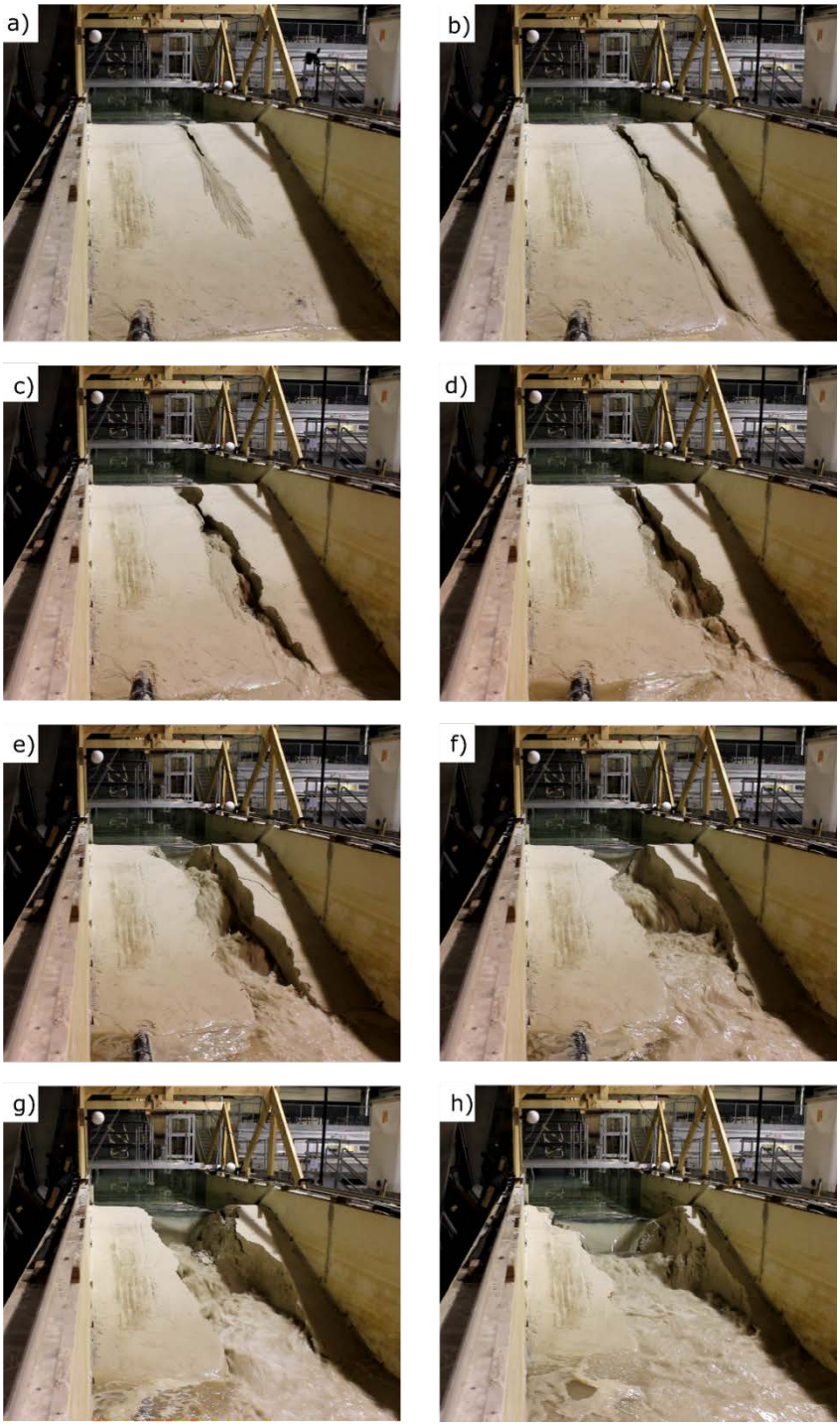

Figure 2.4: Downstream view of dam breach morphology for a typical test. Stage 1 (a-b): an initial channel is incised into the downstream dam face. Stage 2 (c-d): The breach channel forms step like features, retrogressing backward toward the dam crest. Stage 3 (e-h): The breach channel intersects the upstream dam crest, marked by an exponential increase in outflow.

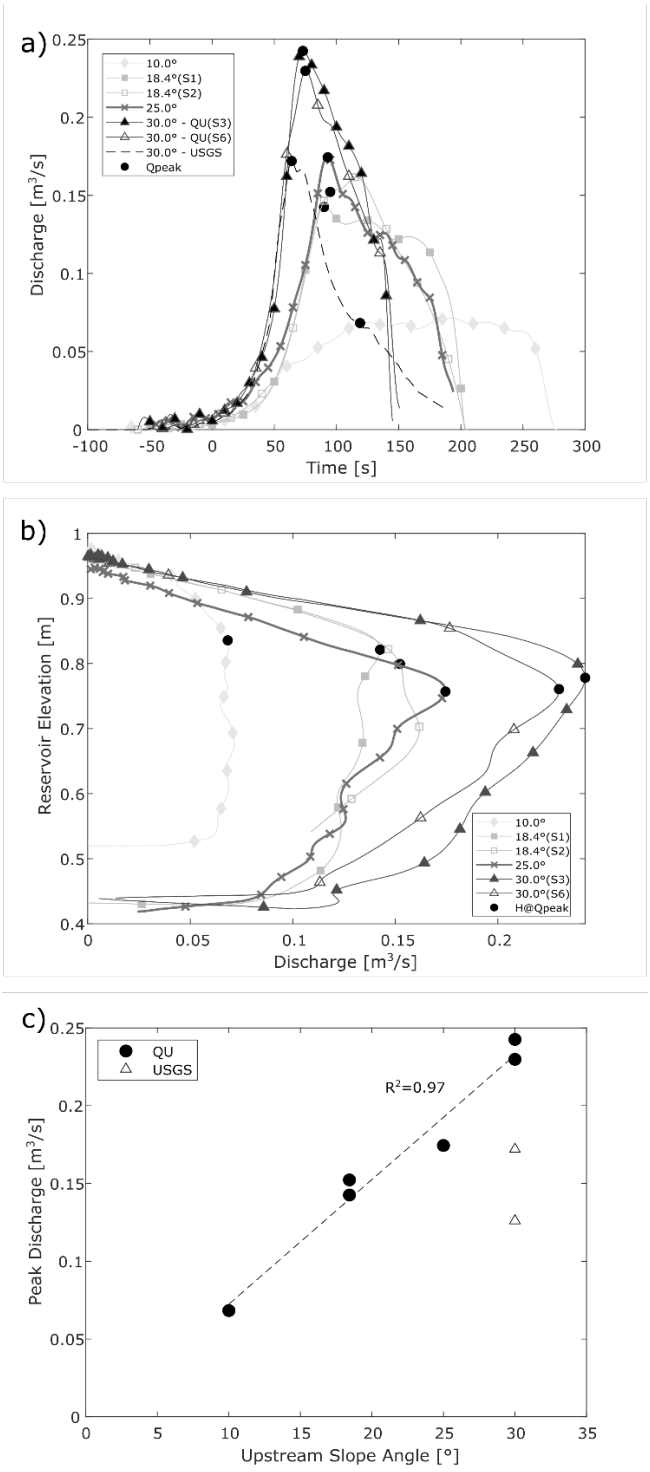

Figure 2.5: a) Breach outflow hydrographs for each test in the series (Discharge vs Time); b) Reservoir Elevation vs Discharge during breach for all tests in the series; c) Peak Discharge vs Dam Upstream Slope Angle. USGS data shown is the high and low range from six test repeats conducted.

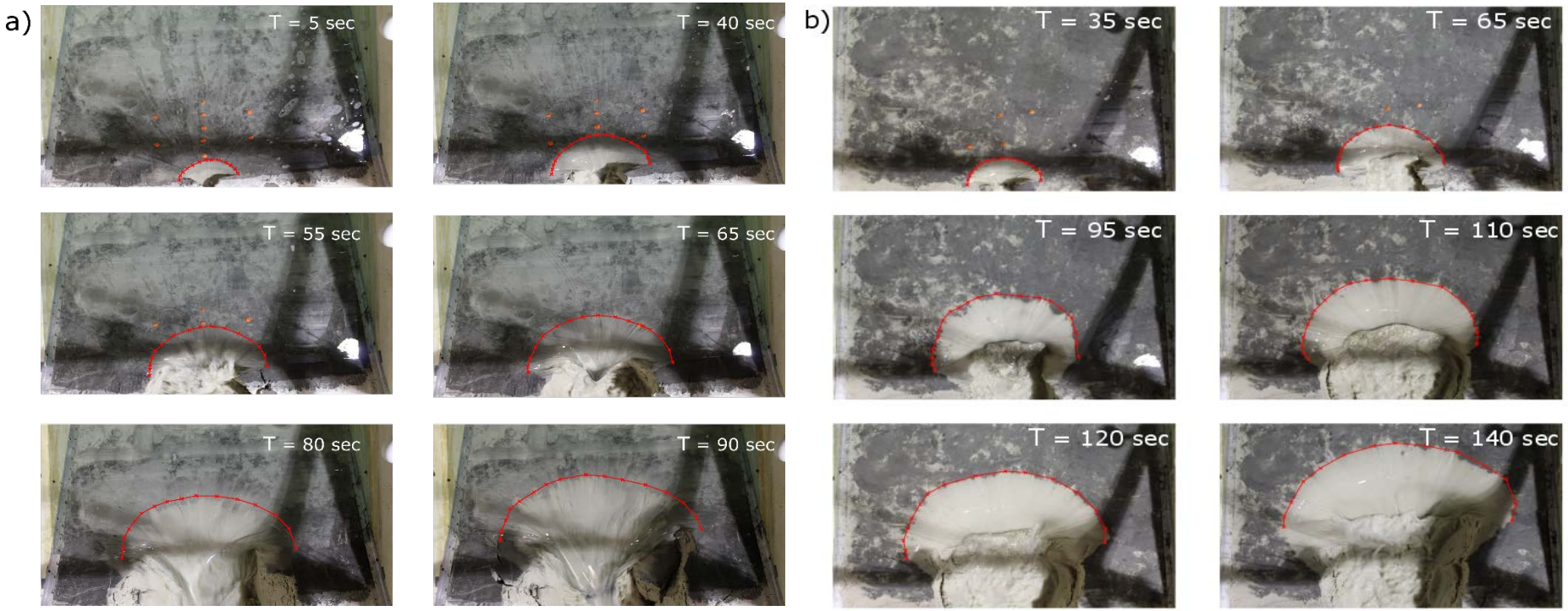

Figure 2.6: a) Plan view of breach growth during a typical test (Test S3). The breach crest shape is visually observed as the boundary of light coloured (eroded) sand and dark colored (intact) sand; b) Plan view of breach crest growth during the 10.0° test. The shape was noted to be more rounded than all other tests, effecting the aspect ratio.

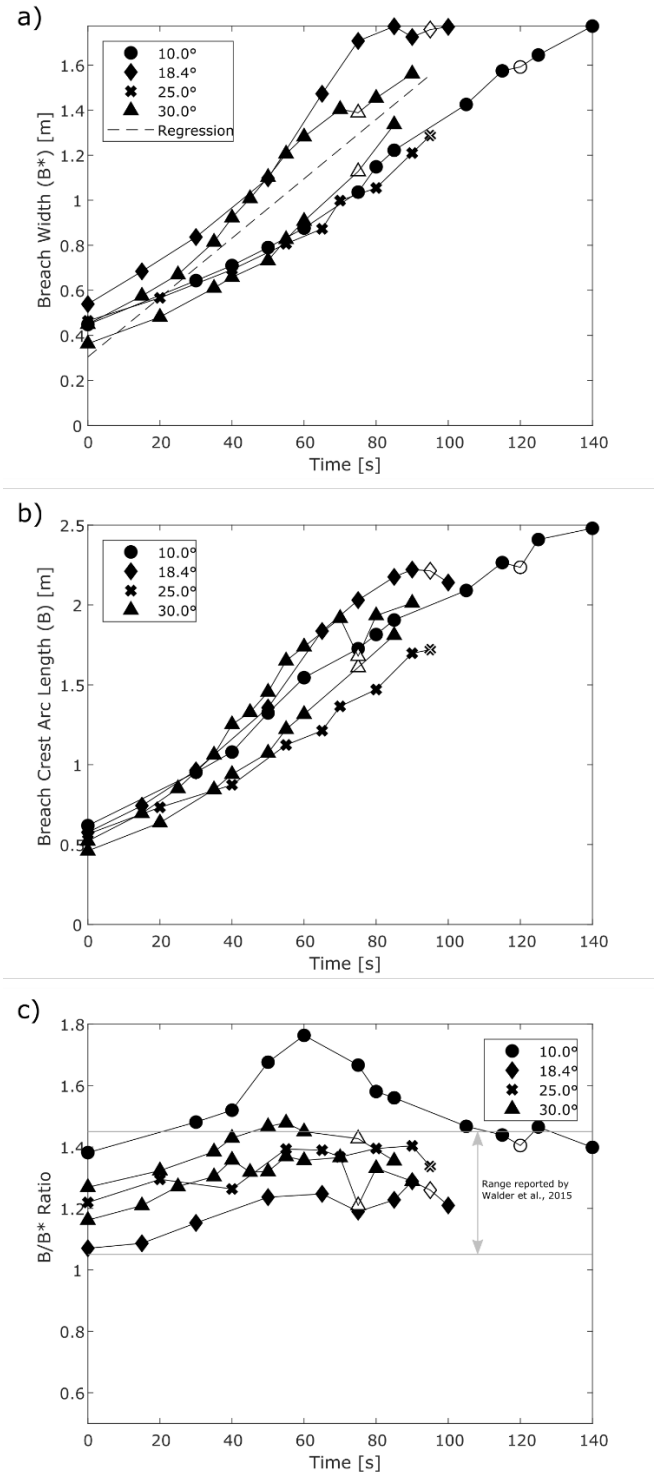

Figure 2.7: a) Horizontal Breach Width (B*) vs Time measured during each test. The white markers indicate peak discharge; b) Breach arc length vs Time measured during each test; c) Ratio of B/B* for each test in the series.

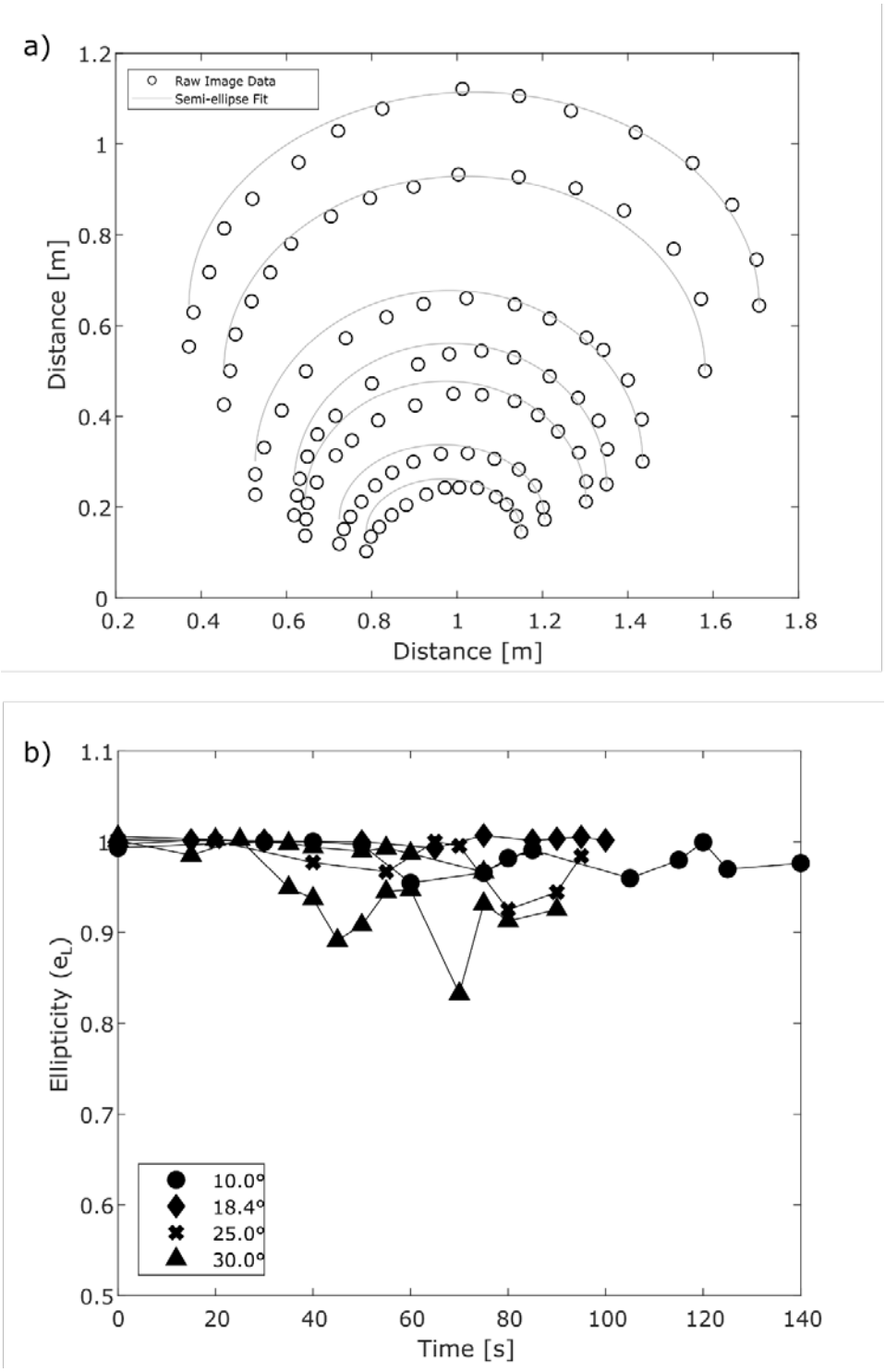

Figure 2.8: a) Example of the ellipticity index calculation; b) Ellipticity index of the breach crest shape, measured during each test, where e_L=1 means the breach crest is perfectly elliptical.

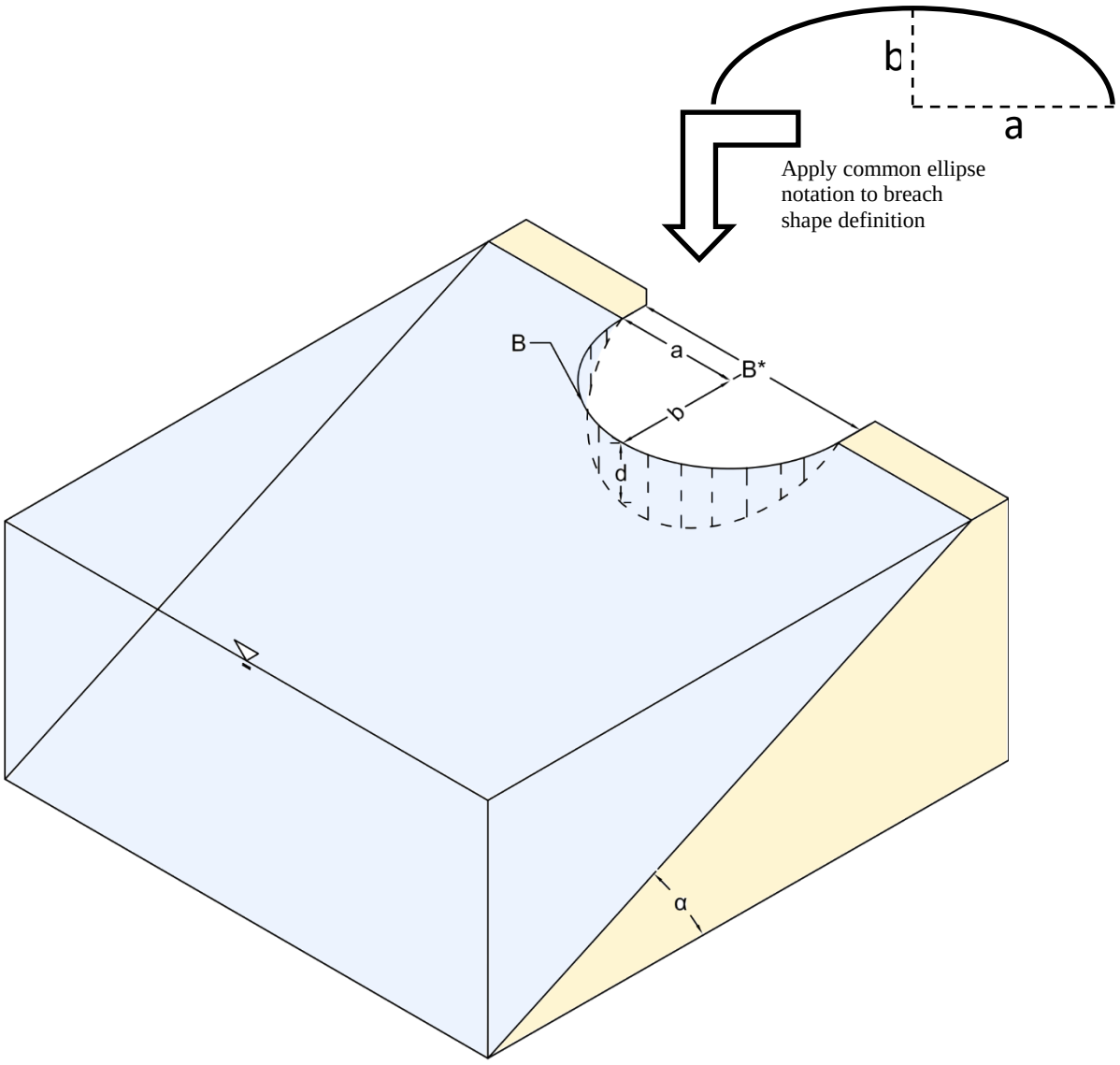

Figure 2.9: Schematic of breach crest, defined by common ellipse notation. The breach crest horizontal distance, B*, equals 2a, where a is the major ellipse axis. The minor ellipse axis, b, measures the horizontal distance from the location where the reservoir elevation intersects the dam height to the breach crest.

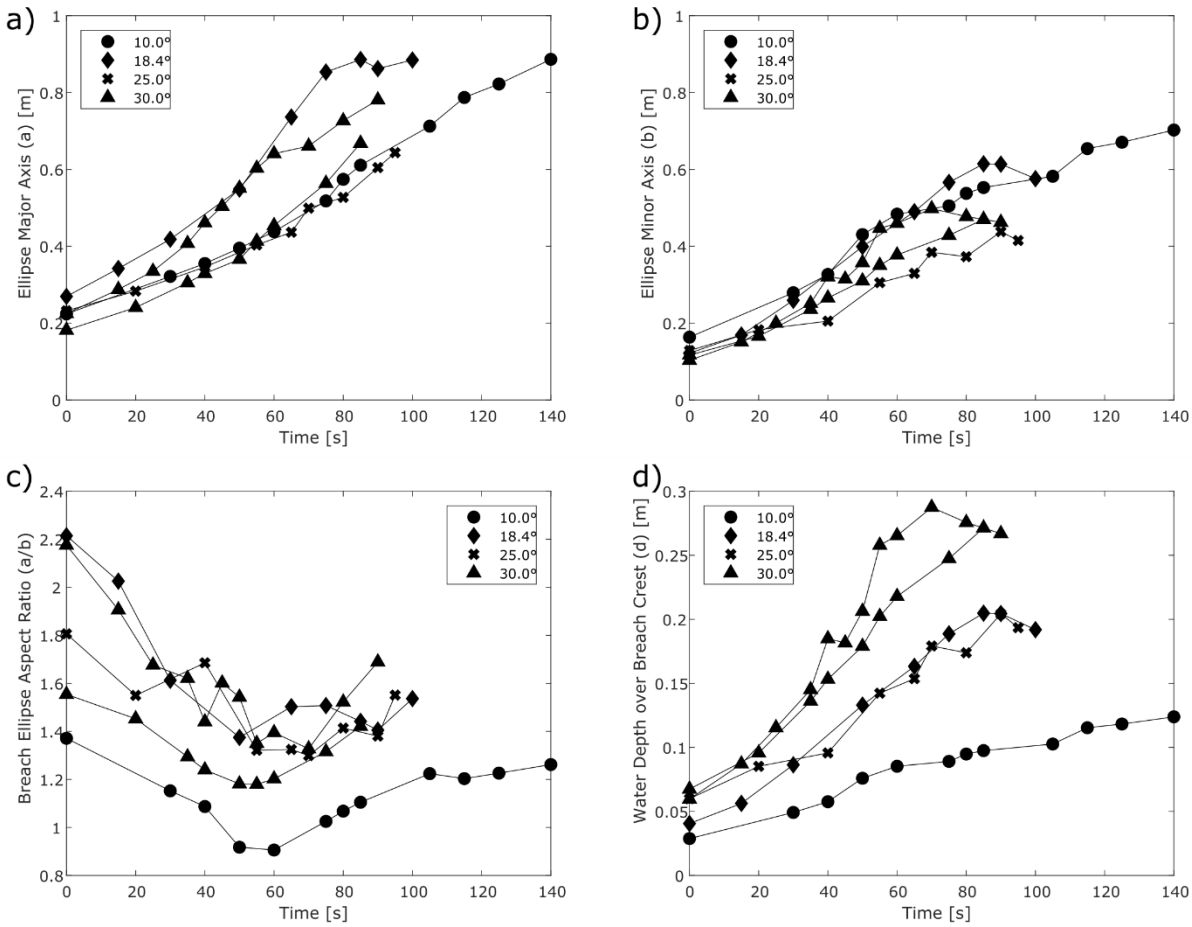

Figure 2.10: a) Ellipse major axis (a) vs Time measured for all tests, where a=B*/2; b) Ellipse minor axis (b) vs Time measured for all tests; c) Aspect ratio (a/b) vs Time for all tests. The average aspect ratio was 1.43; d) Average depth flowing over breach crest (d_{avg}), where d=*xtan(α).**

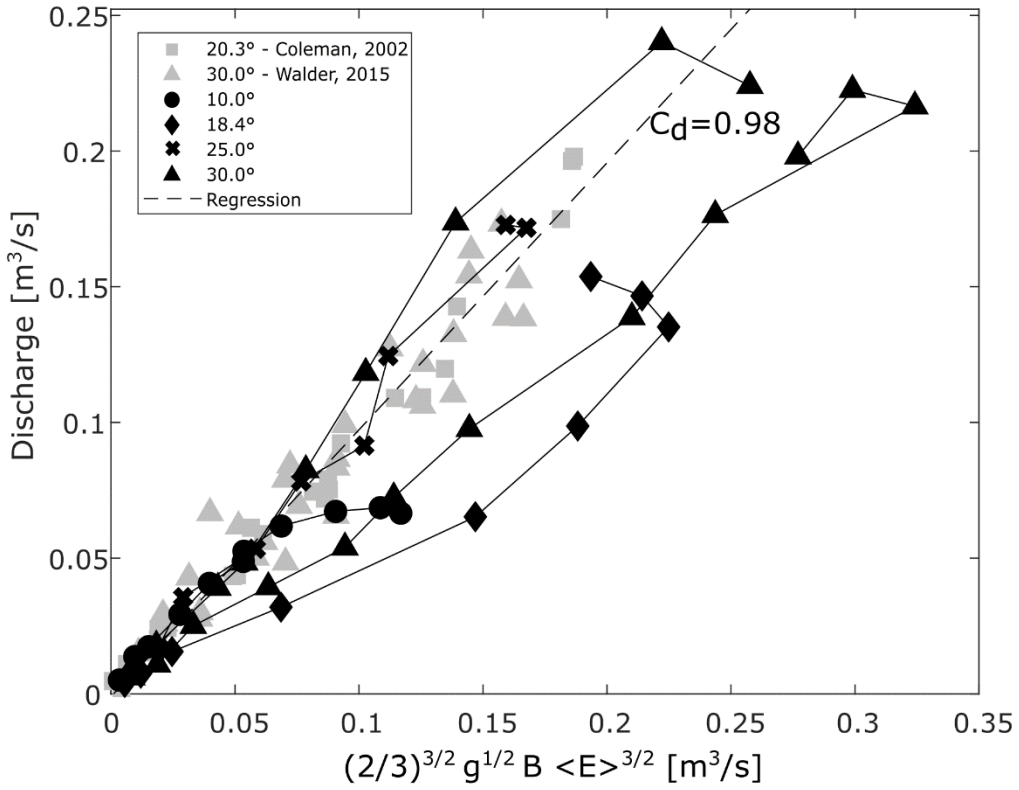

Figure 2.11: Rating curve calculated utilizing the same weir rating curve equation presented by Walder et al. (2015). The grey points show data reported by Walder et al. (2015) and Coleman et al. (2002).

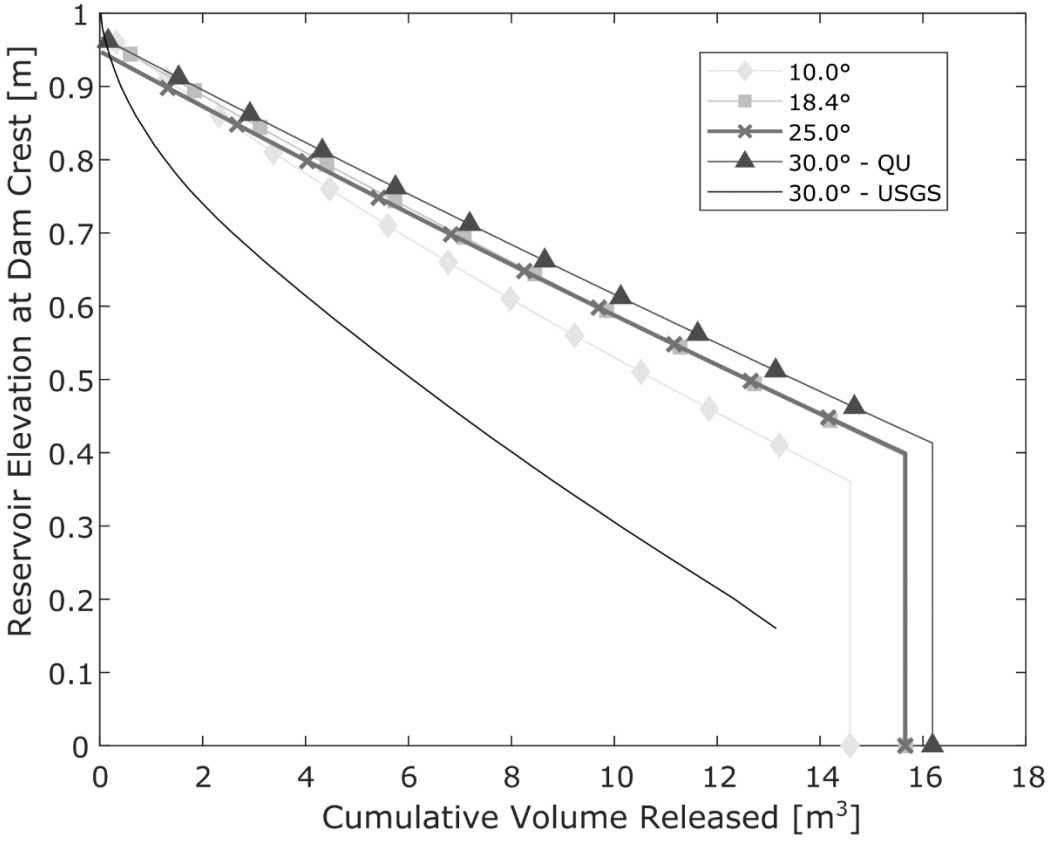

Figure 2.12: Reservoir storage function for each dam in this study, and the storage function reported by Walder et al. (2015). Due to the undersized drain in the downstream deposition area, the deposition area fills during the breach, eventually reaching an equilibrium level with the upstream reservoir.

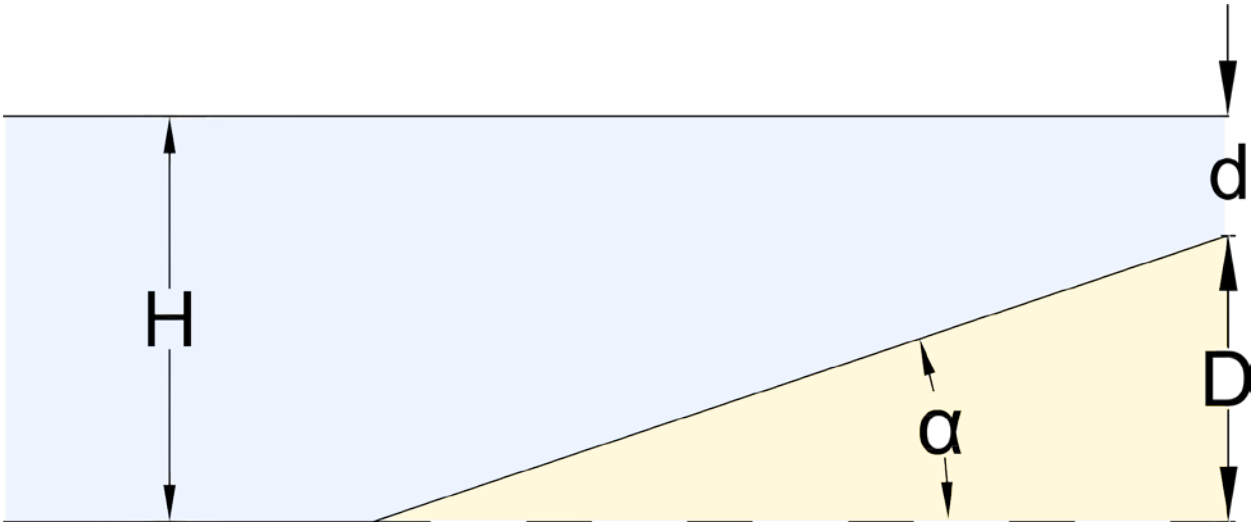

Figure 2.13: Schematic of maximum available discharge condition. The reservoir storage function was shown to limit breach discharge when the reservoir elevation (H) fell below the sum of the dam height below the breach crest location (D) and maximum potential depth of water flowing over the breach crest (d).

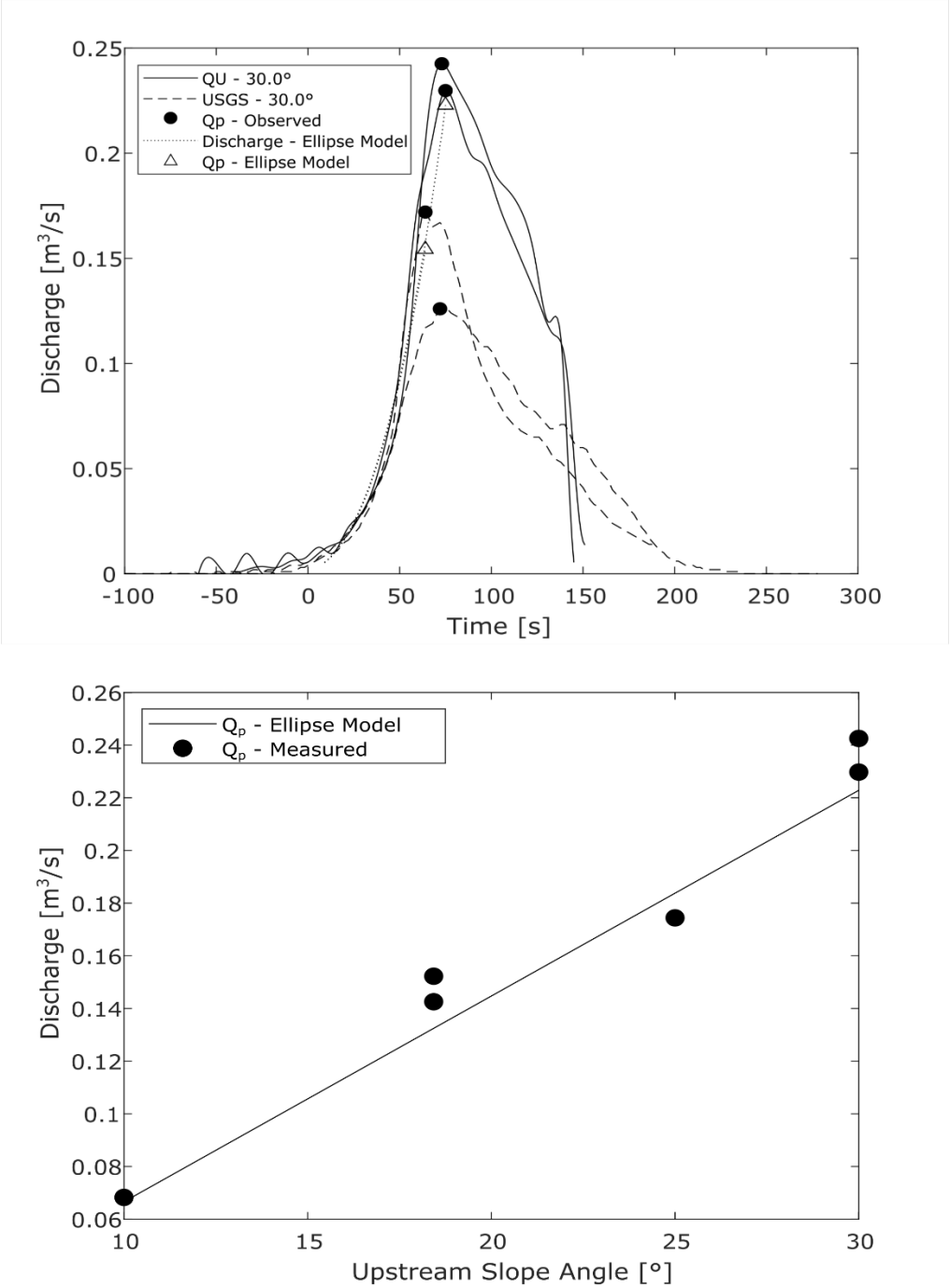

Figure 2.14: a) Discharge model from T=0 to T=peak discharge. The model captures both the dam and reservoir geometry; b) Modelled peak discharge vs upstream slope angle for dams with a range of upstream slope angles tested at the Queen's University laboratory flume

Chapter 3

Effect of beach elevation on peak discharge observed during overtopping of physical model tailings dams

3.1 Introduction

Tailings dam failure is defined by the Tailings Dam Breach Working Group of the Canadian Dam Association (CDA) as “a physical breach of the dam followed by an uncontrolled release of stored materials that could include fluids and tailings” (Martin et al., 2019). Tailings dam breach assessments currently being employed in practice are heavily reliant on methodologies designed for water retaining dams. Considerable research effort has been undertaken to define dam breach processes for water retaining structures including work by Coleman et al. (2002) at the University of Auckland, and Walder et al. (2015) at the United States Geological Survey (USGS) research station in Oregon. These studies were both conducted on breach initiated by overtopping for homogenous, noncohesive embankment dams. In departure from research on dam breach conducted elsewhere, these studies focussed on the arc shaped erosional feature that forms the upstream breach crest, as this was shown to hydraulically control the outflow through the breach, rather than the width of the downstream channel through the dam. In these studies, the breach crest was defined by connecting a series of high points along streamlines flowing over the breach channel where flow is perpendicular to the breach crest at all points along its length (Coleman et al., 2002). Follow on work by Walder et al. (2015) showed that the breach crest is a hydraulic control structure analogous to a weir, separating subcritical flow upstream from supercritical flow downstream, with the volumetric flow rate discharged over the breach crest governed by the size and shape of the breach crest, which evolves dynamically through the breach process.

The shape of the breach crest is defined in these past studies by the breach width horizontal distance, B^*, and the breach arc length, B (Figure 3.1). The depth of water flowing over the breach, d, ranges from zero at the intersection of the breach crest with the reservoir water elevation to its maximum point at the arc apex. As discussed in Chapter 2, a semi-elliptical shape can describe the arc shape of the breach crest throughout failure. The ellipse major axis, a, is equal to $B^*/2$. The minor axis, b, measures the perpendicular distance from the intersection of the breach crest with the reservoir elevation to the breach crest apex. The geometry of tailings dam structures is distinctly different from water retaining dams in a variety of ways, including the presence of tailings beach features combined with a shallow upstream slope angles, which may impact the upstream breach crest evolution and therefore the outflow hydrograph through a breach in the tailings dam case.

A beach is a commonly designed feature in tailings dams, extending from the dam face upstream into the reservoir. At a facility where tailings are deposited from the mineral processing mill in slurry form, shallowly sloping beaches form in the area of the discharge outlet, commonly positioned close to or on the dam crest. In the absence of thickeners or other homogenizing agents, particle segregation occurs as the slurry flow spreads into the reservoir. Denser, coarser grained particles drop out of slurry suspension close to the outlet, while finer grained particles are carried further upstream of the dam, with fluids eventually coming to rest in a supernatant pond (McPhail, 1994). Seepage failure (i.e. piping) is another common dam failure mode. A minimum width of the tailings beach upstream is often specified to maintain a dry distance between the supernatant pond and the dam face. This lowers the hydraulic gradient, reducing the risk of seepage induced failures (Mcleod & Murray, 2003).

The influence of the presence of a tailings beach is hypothesised in Figure 3.2, in which the breach process and outflow hydrograph for a clearwater dam and a tailings dam with a beach are illustrated in Figure 3.2a, and b, respectively. In a clearwater dam, discharge increases rapidly until a peak

point is reached. Peak discharge occurs when the breach crest width and depth flowing over the breach crest reach a maximum combined volume, a function of the geometry of the upstream dam slope and reservoir (Figure 3.2a). However, in a tailings dam with a shallowly sloping beach, the reservoir volume available to flow over the breach crest will be reduced when the breach crest erosion retrogresses beyond the intersection point of the upstream dam slope and the beach. The time during the breaching process that this intersection occurs is important; if the intersection occurs while the discharge rate is still on the rising limb of the outflow hydrograph, then peak discharge will be reduced (Figure 3.2b). However, if peak discharge had already been reached, then the beach cannot have an effect.

The influence of upstream slope angle has already been investigated in Chapter 2, where it was demonstrated that peak discharge is linearly related to the dam upstream slope angle. A steeper upstream slope angle resulted in a deeper flow over the breach crest, leading to a higher peak discharge rate. However, tailings dam slopes are typically constructed with shallower upstream slopes compared to the water retaining dams. Therefore, depth flowing over the breach crest in a tailings dam is expected to be lower, limiting peak discharge.

In this paper, the potential for a tailings beach to impact peak discharge during breach is investigated, specifically if the breach crest intersects the beach while on the rising limb of the outflow hydrograph. Beach features are not found in a traditional water storage facilities, therefore it is imperative to quantify whether this difference in upstream geometry impacts discharge. Five large scale physical model dams, on the other of 1 m in height were constructed, with beach heights ranging from 0.50 m to 0.90 m. In the remainder of this paper we describe the experimental program and show that the previously presented mathematical framework to quantify the instantaneous geometry of the breach crest shape for clearwater dams is also applicable to this case including an upstream beach. Quantitative estimates of peak discharge are made for each beach height tested,

recognizing that the time the breach crest intersects with the beach slope is a determining factor on whether peak discharge is affected by the beach.

3.2 Experimental Methods and Materials

3.2.1 Experimental program

To investigate the effect of shallowly sloping beaches in the upstream reservoir of tailings storage facilities on breach outflow due to overtopping, a test series including five large physical model dams (1.0 m in height) was undertaken. The dams were constructed at the Queen's University Landslide Flume facility, in the 36 m horizontal runout section. Similar to the test series conducted in Chapter 2, the dam crest width, 0.30 m, and downstream dam slope angle, 18.4° (3H:1V), remained constant for all tests. Beach height, measured vertically at the intersection of the beach with the dam upstream slope to the flume base, ranged from 0.50 m to 0.90 m (Figure 3.3). The dam upstream slope angle above the beach intersection was 18.4° in all tests. Details of this test series are presented in Table 3.1, along with two tests, S1 and S2, from Chapter 2, to provide comparison the case of no beach for a dam with an upstream slope angle of 18.4°.

Due to space and material constraints, the length of the beach was terminated at a point located 3 m beyond the original upstream toe location of Tests S1 and S2. To achieve a beach slope angle of 2.9° (5%) over this shortened distance, a vertical cut-off wall at the end of the beach was required. The wall consisted of plywood sheeting, matching the height of the beach at the wall location. The wall was constructed upward sequentially, by adding plywood sections to increase the wall height coinciding with each raise in beach height.

Sliding and overturning were resisted by two 1 m^3 soil bags, each filled with approximately 1000 kg of sand, placed on horizontal straps extending from the wall base upstream into the reservoir.

The vertical cut-off wall also limited the reservoir water volume available during breach. Water in the reservoir below the elevation of the top of the cut-off wall was referred to as “dead volume” since it was obstructed by the wall.

Materials, construction methods, instrumentation and procedures of the clearwater dam test series in Chapter 2 were replicated in their entirety for this test series, with the exception of the addition of the tailings-style beach to the upstream reservoir, to permit a direct comparison between these two cases.

3.2.2 Materials and construction methods

Each dam and beach were constructed entirely from uniform fine sand (#730 Silica Sand by Weldon Company) with a mean grain size, d_{50}, of 0.12 mm. The construction process, highlighting the beach addition, is illustrated in Figure 3.4. The dam structure was constructed in tandem with beach placement. Material from previous tests that was not mobilized downstream of its original location during breach was left in place, while additional sand for subsequent beach raises was added to the flume with a Bobcat skid steer loader. In Test W5, due to the decrease in beach height from Test W4, excess material was removed from the flume prior to construction. A Bobcat excavator was also utilized to move materials deposited downstream in previous tests back to the dam location at the midpoint of the flume horizontal reach (Figure 3.4a). In order to contain the sand in the desired dam geometry, formwork was constructed from plywood sheets. The forms were bolted in place onto aluminum angle brackets, inclined at 18.4° from horizontal for both the upstream and downstream dam slopes, attached to the concrete sidewalls of the flume using anchors. The planned beach height, extending upstream from the intersection point with the dam upstream slope, was marked on each flume side wall at 1 m intervals for a visual guide during placement(Figure 3.4b).

The dam structure was constructed through a combination of hydraulic placement, shovelling and hand tamping. Sand was liquefied into slurry form for hydraulic placement by jetting the sand with high pressure water. The slurry was pumped into place with a Tsurumi HSD 2.55S submersible single-phase portable slurry pump, and a 186 W submersible puddle pump was utilized to evacuate ponded water. The beach structure was constructed by end dumping material into the flume with the Bobcat skid steer, then distributed by hand with a shovel, with limited compactive effort applied by walking on the material (Figure 3.4c).

As in Chapter 2, to avoid the risk of shear failure, a toe drain constructed from two sections of 10.2 cm diameter corrugated high density polyethylene (HDPE) drainage pipe was installed under the dam crest, flush to the flume base and secured to the floor with metal strapping.

Following construction, dams were left to drain for several days prior to removing the formwork. After the formwork was removed, any additional sand required to form the desired shape was shovelled into place, hand tamped and smoothed with a trowel (Figure 3.4d).

3.2.3 Instrumentation

The instrumentation was specifically designed to capture the instantaneous breach crest geometry. This is difficult to capture with images as the height of water changes during the test, causing a variable scale factor between linear distances and pixels due to refraction. Scales were marked on the upstream aluminum angle brackets drilled into the flume side walls, which allowed for calculation of a unique scale factor for each image analyzed that accounted for the difference in refraction as the reservoir water level decreased throughout the breach.

The breach shape evolution was measured on plan view images captured by four Canon EOS Rebel T5 Digital Single-Lens Reflex (DSLR) cameras. The cameras were located at a height of 2.5 m

above the dam crest elevation, positioned over the flume centreline, capturing a combined field of view of approximately 8.0 m in length. These four cameras were synchronized and remotely triggered every 5 seconds during breach.

To consistently delineate the breach crest shape, a thin layer of sand was dyed black with India ink and placed on the surface upstream of the crest. This surficial layer of dark sand contrasted the rest of the light coloured sand of the dam and beach structure. Since the breach crest growth is an erosional process, the breach crest shape could be defined at the boundary of dark (unaffected) and light (eroded) sand.

The reservoir elevation, from which breach discharge can be calculated, was monitored with five Akamina AWP-24 wave capacitance height gauges, distributed longitudinally upstream of the dam along the reservoir centre line, set to a sampling frequency of 100 Hz. One wave height capacitance gauge was also positioned 1.0 m downstream of the dam toe to monitor outflow downstream of the dam.

3.2.4 Test procedure

Following construction of each dam structure, a pre-failure laser scan was completed with a Faro Laser Scanner Focus^{s} 150. Additional laser scans were completed of the downstream deposit and remaining dam/beach structure following failure, gathering data for volume displacement calculations.

A v-notch, approximately 6 cm wide by 6 cm deep, was incised into the centre of the dam crest prior to filling the flume reservoir. The reservoir was filled to the point where water entered the v-notch, initiating overtopping failure. As the first bead of water flowed through the notch and

reached the downstream toe of the dam, data acquisition with the capacitance wave height gauges and plan view cameras was started simultaneously.

During several tests, sediment grab samples were taken downstream of the dam, around the time of peak discharge. The sand and water volumes of each sample were measured in a graduated cylinder and recorded.

3.3 Observations of Dam Breach

3.3.1 Outflow hydrographs

The time rate of outflow during the breach process was calculated utilizing reservoir elevation data captured by upstream wave capacitance gauges, and the geometry upstream of the dam crest. Peak discharge was observed to be similar for dams with beach heights between 0.50 m to 0.72 m, and is comparable to those of clearwater dam tests with the same dam upstream slope angle of 18.4° (Tests S1 & S2 in Chapter 2), ranging from 0.12 m^3/s to 0.16 m^3/s, with a mean peak discharge across these five tests of 0.136 m^3/s, and standard deviation, σ, of 0.015 m^3/s (Figure 3.5a). It is postulated that the differences in observed peak discharge in the tests above is likely due to test to test variability.

In contrast, tests completed with beach heights of 0.80 m and 0.90 m recorded peak discharge values of 0.07 m^3/s and 0.06 m^3/s, respectively. This marked decrease in peak discharge is an important observation in this test series and is investigated further in the remainder of this manuscript.

Another way to visualize breach outflow is to compare reservoir elevation and discharge rate. In each of the 0.80 m and 0.90 m beach height tests, the peak discharge is reached at or slightly above the beach elevation (Figure 3.5b). It was hypothesized that if the beach elevation was intersected

by the reservoir elevation while on the rising limb of the hydrograph (i.e. before peak discharge), then the beach limited water volume available to flow over the breach crest, thereby limiting discharge.

Note that due to the small drain in the depositional zone, the maximum reservoir elevation decrease during breach was limited by the size of the flume downstream of the dam. When the equilibrium water level was reached between the dam reservoir and depositional area, the breach process was halted.

3.3.2 Breach geometry

As described in detail by Walder et al. (2015), the breach crest evolution occurs in three distinct stages. Only the final stage, Stage 3, is of interest in this study. It is marked by the onset of a rapid increase in discharge. This coincides with the time datum, T=0, on the outflow hydrographs presented herein. Similar to Chapter 2, breach geometry throughout failure was measured on plan view images captured at five second intervals during breach. B* and B were measured for a select number of images during failure, between time T=0 and time to peak discharge (Figure 3.6a and b, respectively). For the period of the breach process where data was collected, the breach width and arc length growth rate can be largely described as linear with respect to time, similar to observations in Chapter 2.

The ratio of B/B* is presented in Figure 3.6c. The results observed during this test series were mostly within the range previously reported by Al-Riffai (2014) and Walder et al. (2015) of 1.05 to 1.45.

As demonstrated in Chapter 2, the breach shape throughout failure can be described by a semi-ellipse, with the degree of ellipticity quantified by the ellipticity index:

$$e_B = 1 - 2\frac{A_B - A_{B\cap E}}{A_B} \qquad (1)$$

where:

e_B = breach semi-ellipticity index

A_B = original breach area

$A_{B\cap E}$ = area of geometrical intersection between original breach shape and its idealized elliptical shape

A perfect fit would be where the area of the breach exactly overlaps with the area of an ellipse, $A_B = A_{B\cap E}$, so $e_B = 1$. The measured degree of semi-ellipticity of the dam breach crest was generally greater than 0.95, so a semi-ellipse shape can also describe the shape of the dam breach crest in this test series very well (Figure 3.7).

When a semi-ellipse is fit to the breach shape, the major axis a, aligns with the breach width, B*, where a=B*/2. Based on the method by Ramanujan (1914), the perimeter of the semi-ellipse (breach crest arc length) is approximately equal to:

$$B \approx \frac{\pi\left[3(a+b) - \sqrt{(3a+b)(a+3b)}\right]}{2} \qquad (2)$$

As shown in Figure 3.8a and b, the growth rates of ellipse parameters a and b were largely linear, as be expected as they are a function of B*, which was shown earlier increase linearly with time.

The aspect ratio, a/b, describes the proportional relationship between the major and minor axis of the ellipse (Figure 3.8c). The mean value of a/b for was 1.31 ± 0.23, ranging from about 0.87 to 1.84 across all tests. Though a/b was variable throughout the failure, it was observed to be somewhat constant between 0 seconds to 50 seconds in all tests, with a mean value of about 1.4. Image analysis during breach was ended at the time peak discharge, at about 100 seconds after the start of Stage 3.

From geometry, the depth flowing over the breach crest can be determined at any point along the crest by:

$$d = x * tan\alpha \qquad (3)$$

where:

d = depth over breach (m)

x = perpendicular distance from point of water surface intersection with upstream dam face to breach crest (m)

α = upstream slope angle (°)

From Equation (3), the depth flowing over the breach crest is a function of the upstream dam geometry, inclusive of the beach geometry. When the breach crest intersects the inflection point between the upstream dam slope and the beach, transitioning from a slope angle from 18.4° to 2.9°, depth is reduced (Figure 3.8d). However, upstream slope angle alone cannot be used to calculate peak discharge, as discussed in Chapter 2. The behaviour observed in this test series indicated that in addition to the change in slope angle at the breach-beach intersection, the timing of this

intersection was important in determining whether the presence of the beach affected peak discharge. If the intersection of the beach occurs while the breach process is on the rising limb of the hydrograph (Figure 3.5a), then the beach essentially starves the breach process of water by limiting the depth available to flow over the breach crest and drive the erosional breaching process. On the contrary, if the beach is not intersected by the breach crest before peak outflow is reached, then the beach was not observed to have a meaningful effect on peak discharge.

3.3.3 Rating Curve

The methods for calculating discharge during breach were identical to those presented in Chapter 2, with the exception of test data from this series being utilized to evaluate the discharge coefficient, C_d.

The discharge equation to describe flow over the breach crest employed by Walder et al. (2015) was:

$$Q = C_d \left(\frac{2}{3}\right)^{3/2} g^{1/2} B < E >^{3/2} \qquad (4)$$

where:

Q = discharge (m^3/s)

C_d = discharge coefficient (dimensionless)

g = acceleration due to gravity (m/s^2)

B = breach crest arc length (m)

<E> = mean specific energy (m)

At an average depth along the breach crest, d_{avg}, <E> can be written as:

$$< E >= \frac{v^2}{2g} + d_{avg} \qquad (5)$$

where:

v = mean flow velocity (m/s)

d_{avg} = average depth flowing over breach crest (m)

The Froude number is a hydraulic relationship of the ratio of gravitational forces to inertial forces, and provides a method of classifying flow conditions, defined as:

$$Fr = \frac{v}{\sqrt{g * d_{avg}}} \qquad (6)$$

where:

Fr = Froude number (dimensionless) (Yalin & Da Silva, 2001)

The breach crest has previously been described as the location of critical flow, separating upstream subcritical flow and downstream supercritical flow. Due to the strong curvature of the streamlines at the breach crest, relationships for steady, uniform, rectangular flow cannot be applied to the elliptically shaped weir, specifically, the critical Froude number does not equal 1 at this location (Castro-Orgaz & Chanson, 2009). Walder et al. (2015) calculated the critical Froude number at the breach crest to be 0.74 ±0.14 utilizing laboratory data. Assuming that the Froude number at the breach crest in this study is similar, due to comparable dam dimensions and materials, Fr=0.74 can be substituted into Equation (6) to solve for the average flow velocity, and Equation (5) can be re-written as:

$$< E >= 1.274 d_{avg} \qquad (7)$$

A rating curve was plotted to evaluate the fit of the discharge equation to lab measurements in this test series, comparing measured outflow to the outflow calculated utilizing Equation (4) (Figure 3.9). This plot also includes data presented by Walder et al. (2015). Any points occurring after the marked decrease in depth flowing over the breach crest were omitted from the rating curve, with the intention of only describing breach behaviour from time T=0 to the time of peak discharge. The slope of the rating curve is equal to the discharge coefficient, C_d. C_d is a correction factor, calculated post-test to account for difference in measured discharge and ideal calculated values. The C_d value for this test series was found to be 0.89, which is lower than observed in Chapter 2 and that reported by Walder et al. (2015) of 0.98 and 0.96, respectively. However, the data from the 0.65 m beach test does not fit well with the other tests in this series, potentially due to over calculation of depth flowing over the breach crest due to possible variation in post impoundment geometry from the design geometry. If this test is omitted from the calculation, Cd=0.96. In model calculations, a C_d=0.98 was utilized, with the rational of conservatively overestimating peak discharge, and for a direct comparison to Chapter 2 results.

The rating curve suggests that the outflow equation presented by Walder et al. (2015) is a good method to describe outflow for a semi-elliptically shaped breach crest, prior to breach-beach intersection.

3.3.4 Peak outflow model

As discussed in Section 3.3.2, the dam upstream slope angle alone could not describe peak outflow. Available reservoir storage volume was also found to be an important factor in Chapter 2. The shape of the reservoir storage function for each dam in the test series was unique due to the variable height of the beach. The total volume available for released during breach ranged from was about 10.25 m^3 for a beach height of 0.90 m to roughly 16 m^3 for the case of no beach (Figure 3.10).

To model breach outflow based on the framework of a semi-elliptical breach crest shape, a general breach crest growth rate, based on a linear regression of B* vs time, shown on Figure 3.6a, was incorporated into the discharge equation presented by Walder et al., 2015. The aspect ratio of the breach crest was taken as 1.4, the approximate mean value before the beach started to interact with the breach crest. The depth flowing over the weir can be calculated on an iterative basis, by tracking the breach crest location as it retrogresses upstream. When the breach crest shape surpasses the intersection of the upstream dam slope and the beach slope, the depth flowing over the breach begins to decrease. Simultaneously, the discharge iteration also monitors the reservoir elevation, which decreases for each timestep based on calculated discharge and compares to the modelled depth over the breach crest and dam structure elevation. Peak discharge is affected by the presence of the beach only if the breach crest interacts with the beach slope before the peak discharge condition is reached. That is to say, for the given reservoir and dam geometry, there is a specific discharge volume that is required to reach peak discharge. Since the beach limits volume available to the breach process, if this peak discharge volume has not been released prior to beach intersection, then the beach will limit peak discharge.

The method described above can used to reasonably calculate the peak discharge rate and time to peak for dams constructed with beaches of height 0.50m to 0.72 m (Figure 3.11a), 0.80 m (Figure 3.11b) and 0.90 m (Figure 3.11c). The model estimation compared to peak discharge measurement for the 0.90 m test did not agree as well as the other cases. Standard deviation, σ, was calculated for peak discharge for the population of dams with an 18.4° upstream slope angle, and beach height between 0.00 m to 0.72 m (Tests S1, S2, W1, W2 &W5). Standard deviation was 0.017 m^3/s. When this is considered along with the ellipse model fit for the 0.90 m case, the modelled result and measured peak discharge comes within $\pm\sigma$.

The quality of the ellipse model fit, and the effect of the breach-beach interaction, can also be visualized as peak discharge compared to the depth to beach from the maximum reservoir elevation, where the semi-elliptical model results and the measured peak discharge are bounded in the grey area (Figure 3.12).

3.4 Conclusions

Five large-scale physical model tests of 1.0 m high dams with upstream beach elevations ranging from 0.5 m to 0.9 m were tested to define the effect of beach elevation on breach peak discharge. The results of these tests quantitatively confirm the hypothesis that the presence of at tailings-style beach in the dam reservoir impacts peak discharge only if the breach crest intersects the beach slope while the discharge rate is on the rising limb of the outflow hydrograph. Peak discharge rates for beach heights less than 0.80 m were similar to those for clearwater dam Tests S1 and S2 in Chapter 2. However, when the beach height exceeded 0.80 m, peak discharge was reduced by almost 50%, from about 0.14 m^3/s to less than 0.07 m^3/s.

The semi-elliptical fit peak discharge calculation presented provided reasonable estimations of peak discharge. The model utilized a linear breach growth rate and constant ellipse aspect ratio to iteratively determine peak discharge based on upstream geometry, occurring when the erosional breach process became water limited, either due to reservoir geometry or beach intersection.

This work focussed on breach by overtopping, initiated with a v-notch cut in the dam crest along the flume centreline. Other failure modes, such as shear failure, would result in different discharge relationships and warrant further research. In this study, materials did not experience flow liquefaction during failure. Post-peak outflow calculations were not included due to the test flume boundary conditions, restricting data collection.

3.5 References

Al-Riffai, M. (2014). *Experimental Study of Breach Bechanics in Overtopped Noncohesive Earthen Embankments*. University of Ottawa.

Castro-Orgaz, O., & Chanson, H. (2009). Bernoulli theorem, minimum specific energy, and water wave celerity in open-channel flow. *Journal of Irrigation and Drainage Engineering*, *135*(6), 773–778. https://doi.org/10.1061/(ASCE)IR.1943-4774.0000084

Coleman, S. E., Andrews, D. P., & Webby, M. G. (2002). Overtopping breaching of noncohesive homogeneous embankments. *Journal of Hydraulic Engineering*, *128*(9), 829–838. https://doi.org/10.1061/(ASCE)0733-9429(2002)128:9(829)

Martin, V., Al-Mamun, M., & Small, A. (2019). CDA technical bulletin on tailings dam breach analyses. *Sustainable and Safe Dams Around the World*, *d*, 3484–3498. https://doi.org/10.1201/9780429319778-313

Mcleod, H. N., & Murray, L. (2003). Tailings Dam Versus a Water Dam, What is the Design Difference? *ICOLD Symposium on Major Challenges in Tailings Dams*, 1–12.

McPhail, G. (1994). *Prediction of the Beaching Characteristics of Hydraulicaly Placed Tailings*. University of Witwatersrand, Johannesburg, South Africa.

Walder, J. S., Iverson, R. M., Godt, J. W., Logan, M., & Solovitz, S. A. (2015). Overtopping of Noncohesive Earthen Dams. *Water Resources Research*, *51*, 6701–6724. https://doi.org/10.1002/2014WR016620.Received

Yalin, S., & Da Silva, A. M. F. (2001). *Fluvial Processes*. Delft, The Netherlands: International Association of Hydraulic Engineering and Research.

Table 3.1: Beach Height Test Series Details

Test ID	Dam Height (m)	Reservoir Elevation at Breach (m)	Dam Crest Breadth (m)	Dam Width (m)	Upstream Slope (°)	Downstream Slope (°)	Pilot Notch Location	d_{50} (mm)	Beach Height (m)	Cut-off Wall Height (m)	Q_{peak} (m^3/s)
W1	1.00	0.93	0.30	2.10	18.4	18.4	Flume Centre	0.12	0.50	0.28	0.12
W2	1.00	0.96	0.30	2.10	18.4	18.4	Flume Centre	0.12	0.65	0.40	0.12
W3	1.00	0.94	0.30	2.10	18.4	18.4	Flume Centre	0.12	0.80	0.53	0.07
W4	1.00	0.98	0.30	2.10	18.4	18.4	Flume Centre	0.12	0.90	0.61	0.06
W5	1.00	0.99	0.30	2.10	18.4	18.4	Flume Centre	0.12	0.72	0.45	0.14
S1	1.00	0.96	0.30	2.10	18.4	18.4	Flume Centre	0.12	0.00	0.00	0.14
S2	1.00	0.97	0.30	2.10	18.4	18.4	Flume Centre	0.12	0.00	0.00	0.16

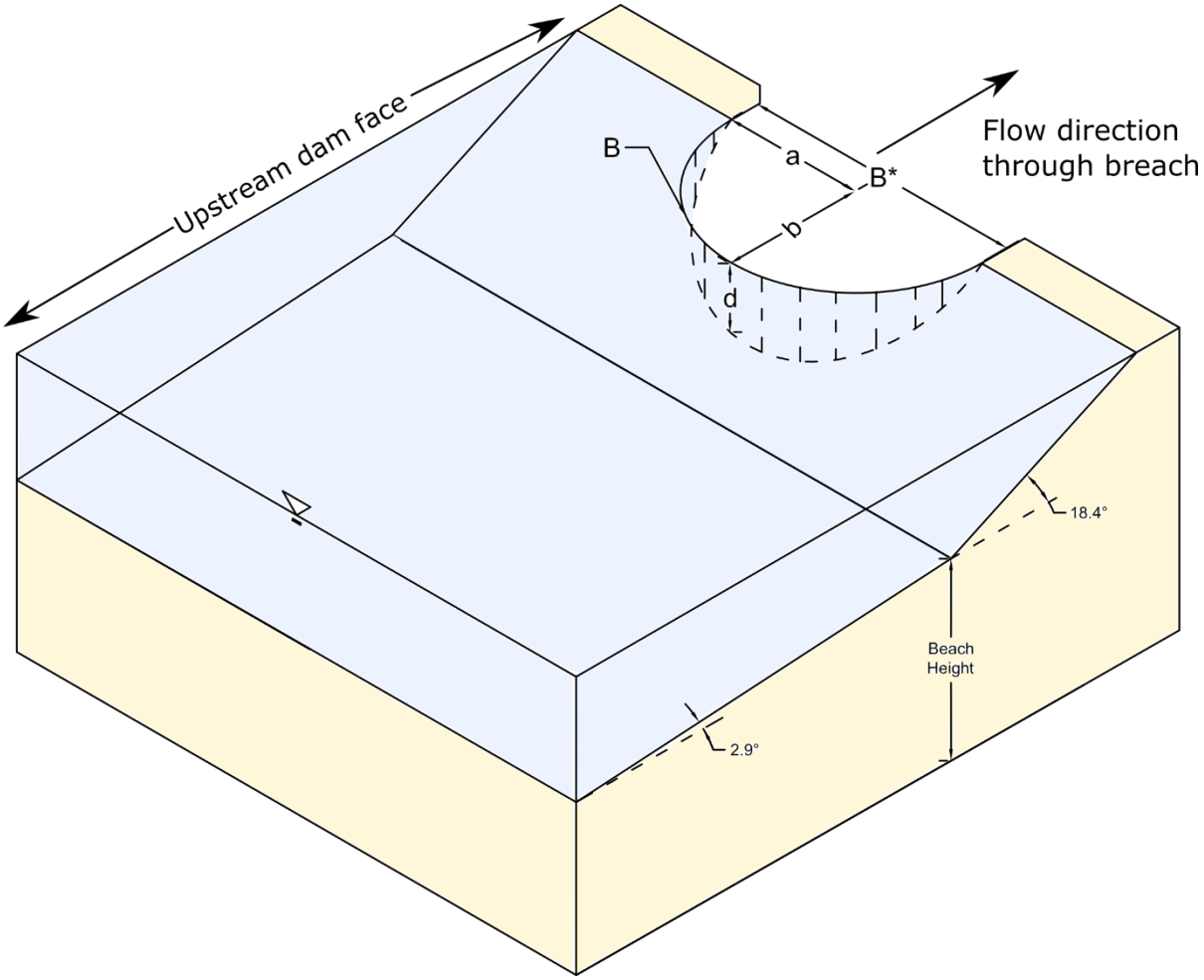

Figure 3.1: Breach geometry definition sketch

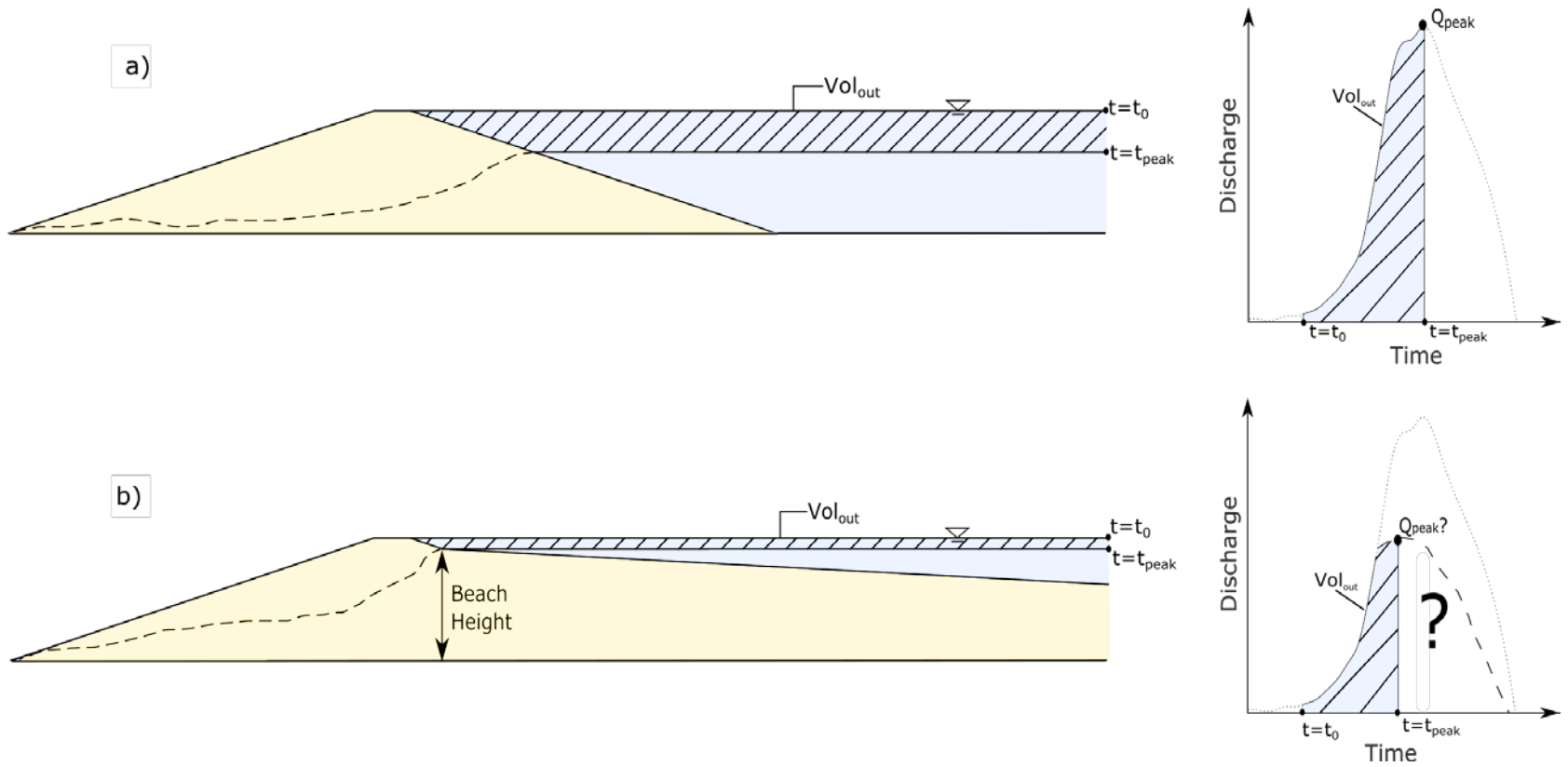

Figure 3.2: Reservoir geometry peak discharge condition for: a) water retaining dam; b) dam with a tailings-style beach. Developing a revised peak discharge condition to describe the effect of a beach on peak discharge is the main subject of this paper.

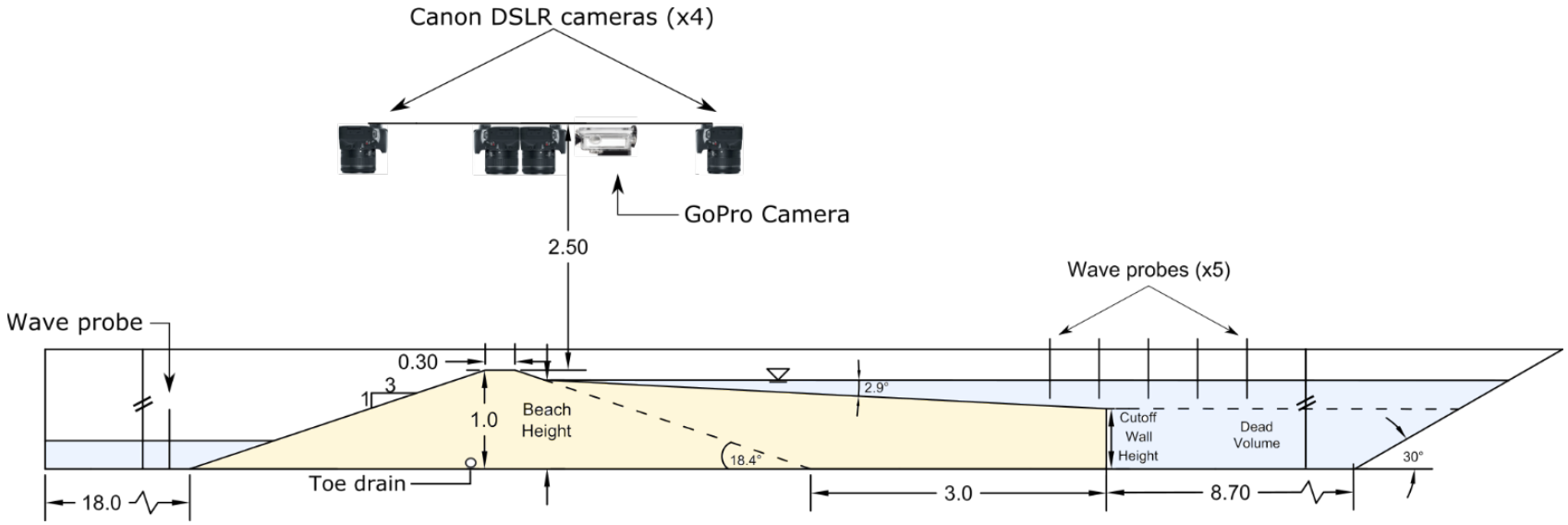

Figure 3.3: Test series instrumentation layout

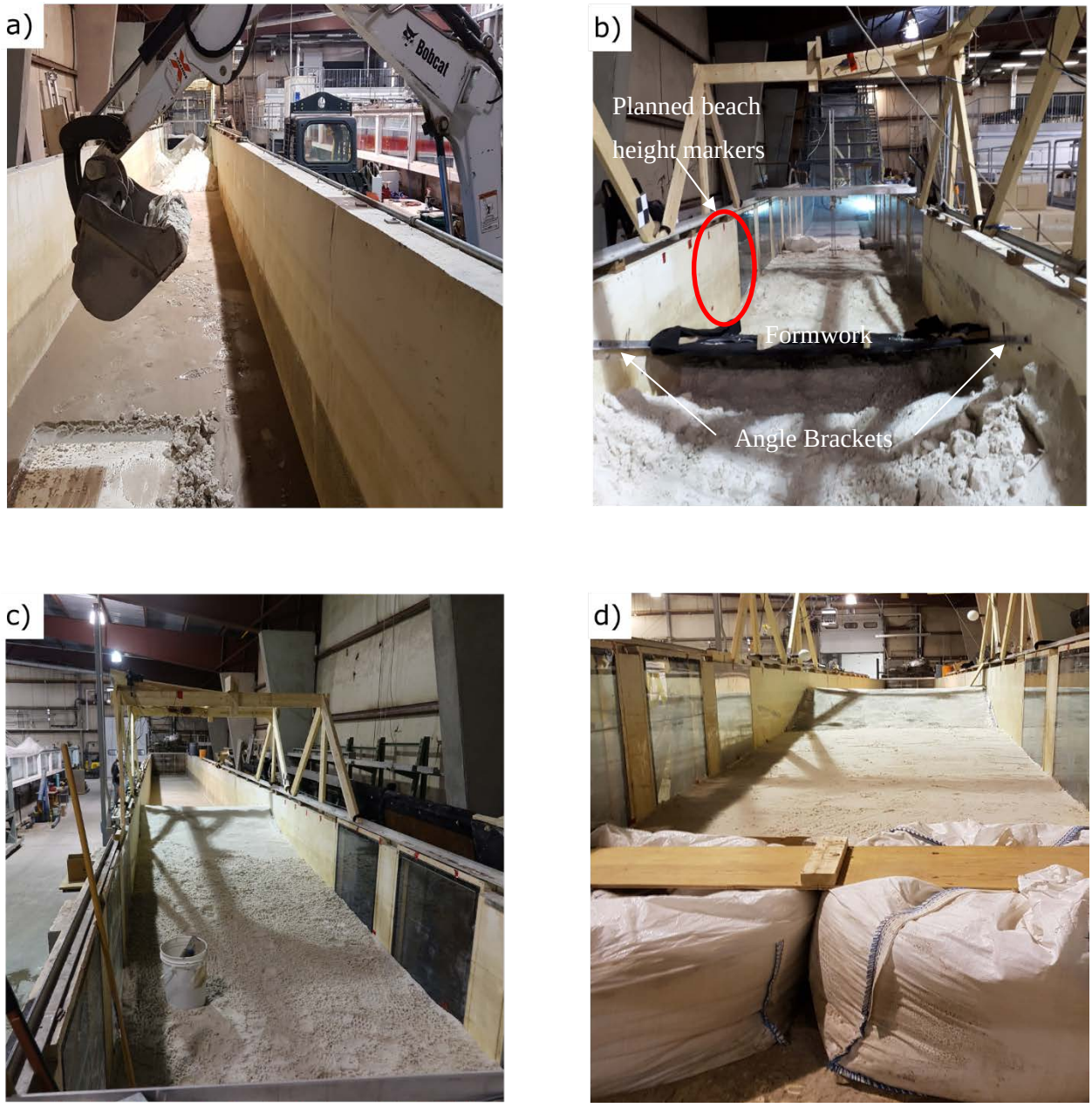

Figure 3.4: Beach construction images. a) Excavation of material deposited during previous breach trial; b) Dam and beach structure construction – formwork in place on upper portion of dam slope, beach construction occurring below form piece; c) Dam and beach structure nearing end of construction; d) Looking downstream from behind the beach cut-off wall, formwork removed, and dyed sand place on upper portion of upstream slope for image analysis.

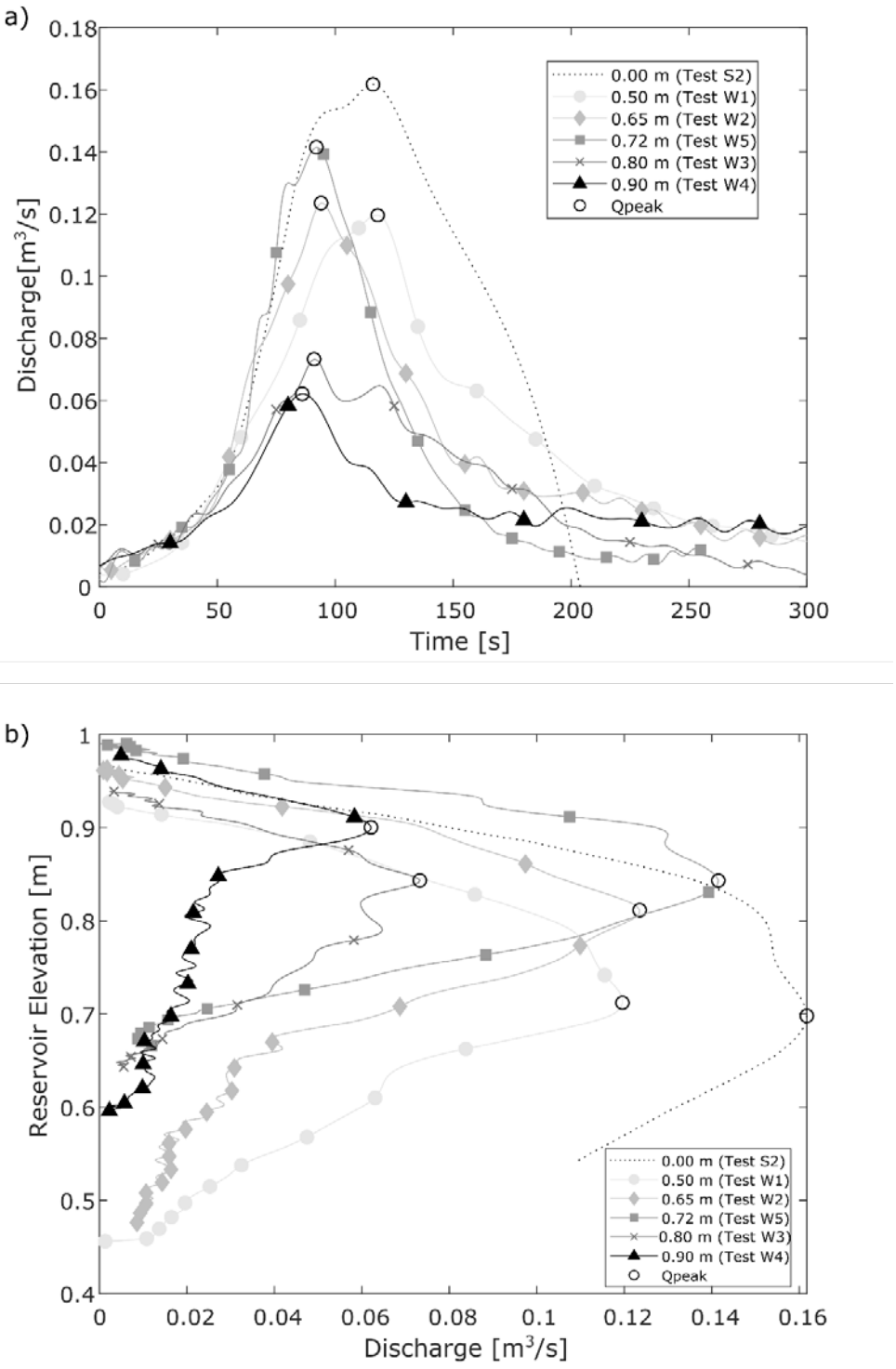

Figure 3.5: Breach outflow hydrograph. a) Discharge vs time during breach. T=0 is the time of exponential increase in discharge; b) Reservoir elevation vs discharge rate

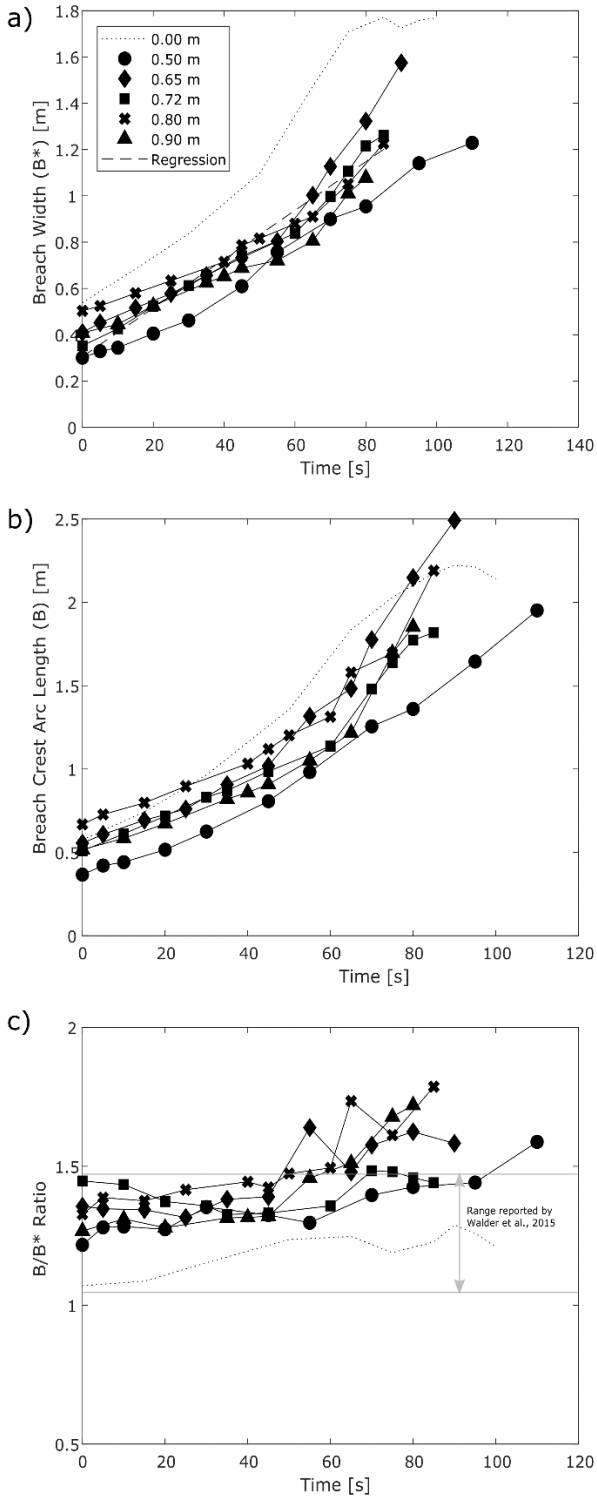

Figure 3.6: Breach crest growth throughout failure. a) Horizontal breach crest length (B*); b) Breach arc length distance (B); c) Ratio of B/B*

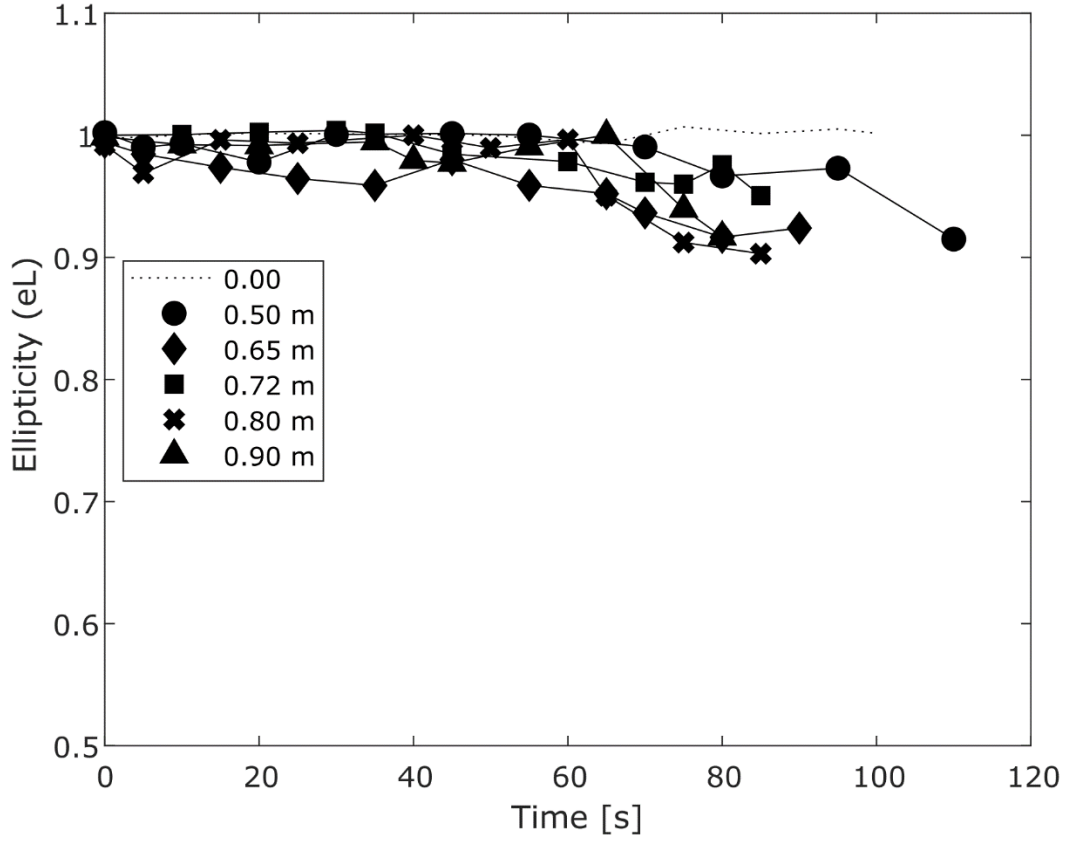

Figure 3.7: Ellipticity index throughout failure, a measure of how well a semi-ellipse fits the breach crest shape. Where e_L=1, the semi-ellipse fit is perfect, so it is a very good fit for this test series.

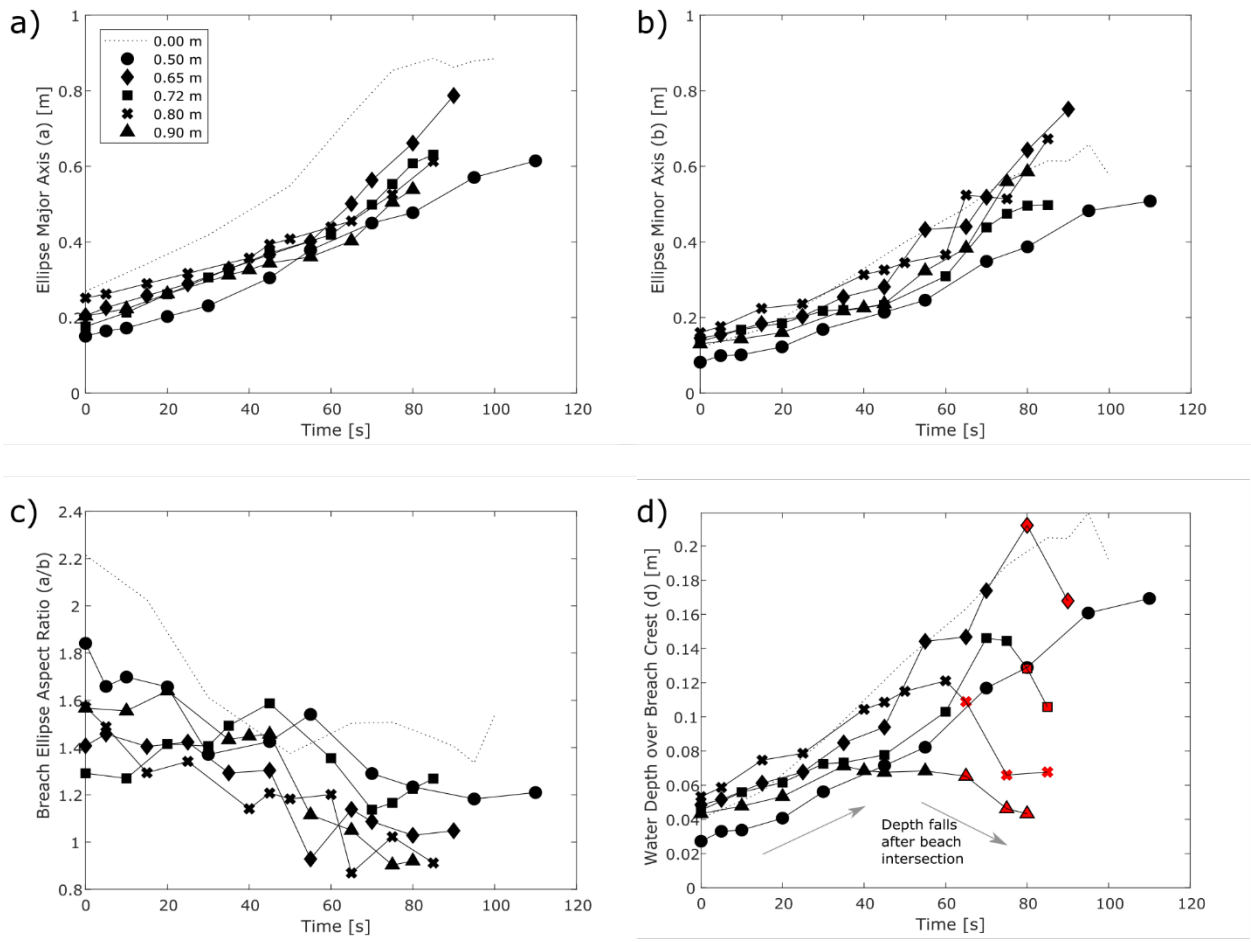

Figure 3.8: Breach parameters in semi-ellipse geometry terms a) Length of Ellipse major axis, a; b) Length of ellipse minor axis, b; c) Aspect ratio of ellipse shape (a/b); d) Average depth flowing over breach crest (d_{avg}). When breach crest shape starts to interact with shallow beach slope, the depth flowing over the breach crest is reduced. These occurrences are marked in red.

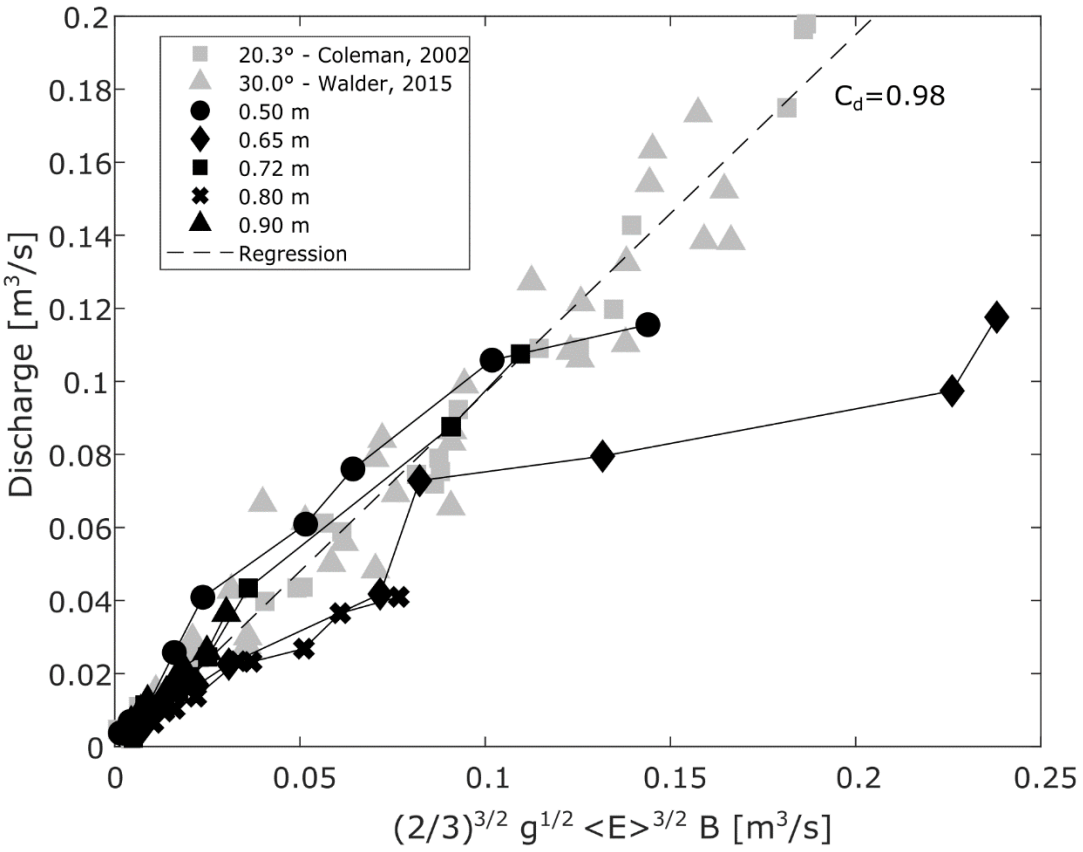

Figure 3.9: Rating curve for breach discharge, based on equation presented by Walder et al., (2015)

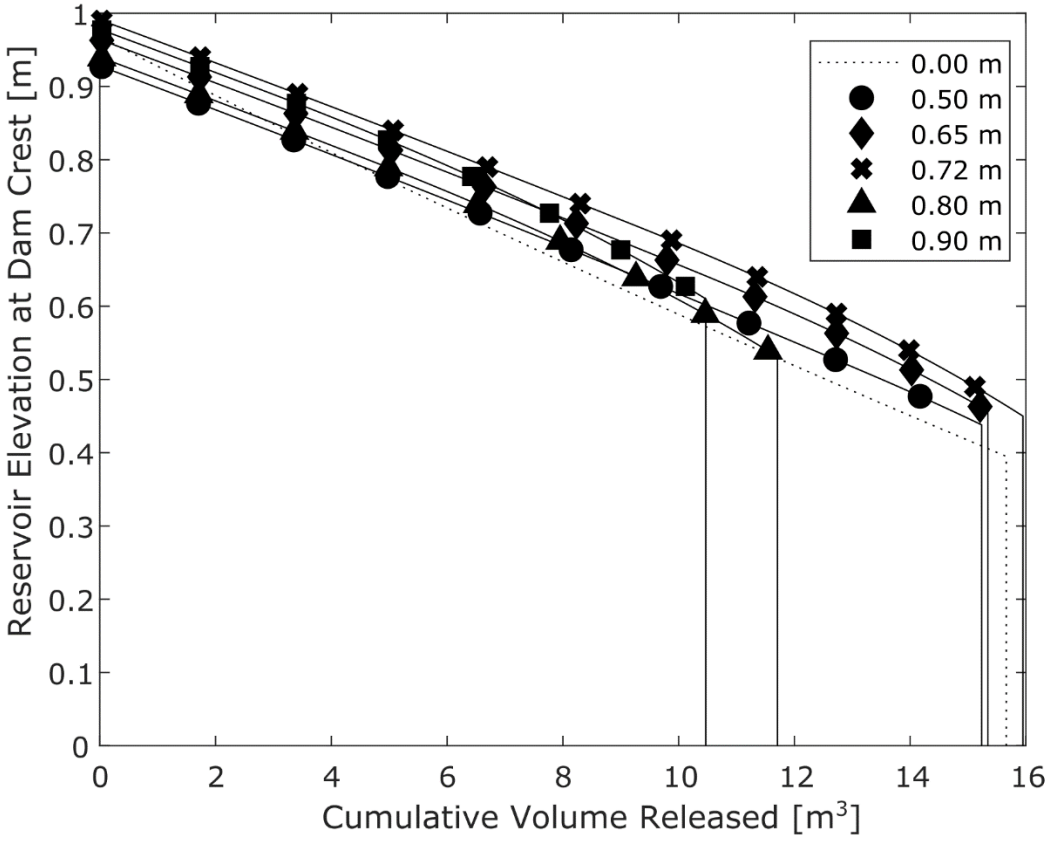

Figure 3.10: Reservoir storage function for each beach height in the test series

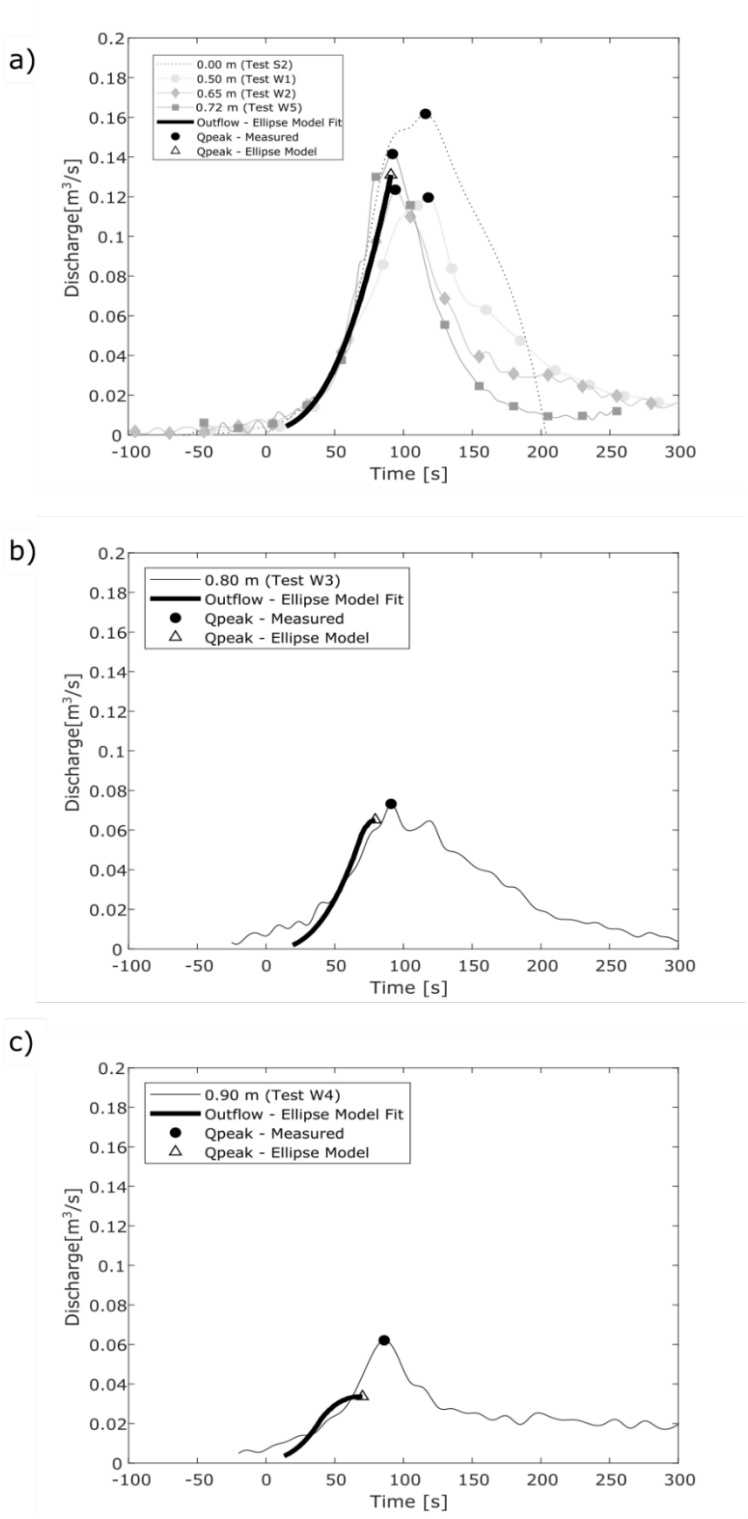

Figure 3.11: Semi-ellipse model fit compared to measured data. a) Tests with beaches lower than 0.80m; b) 0.80 m beach height; c) 0.90 m beach height

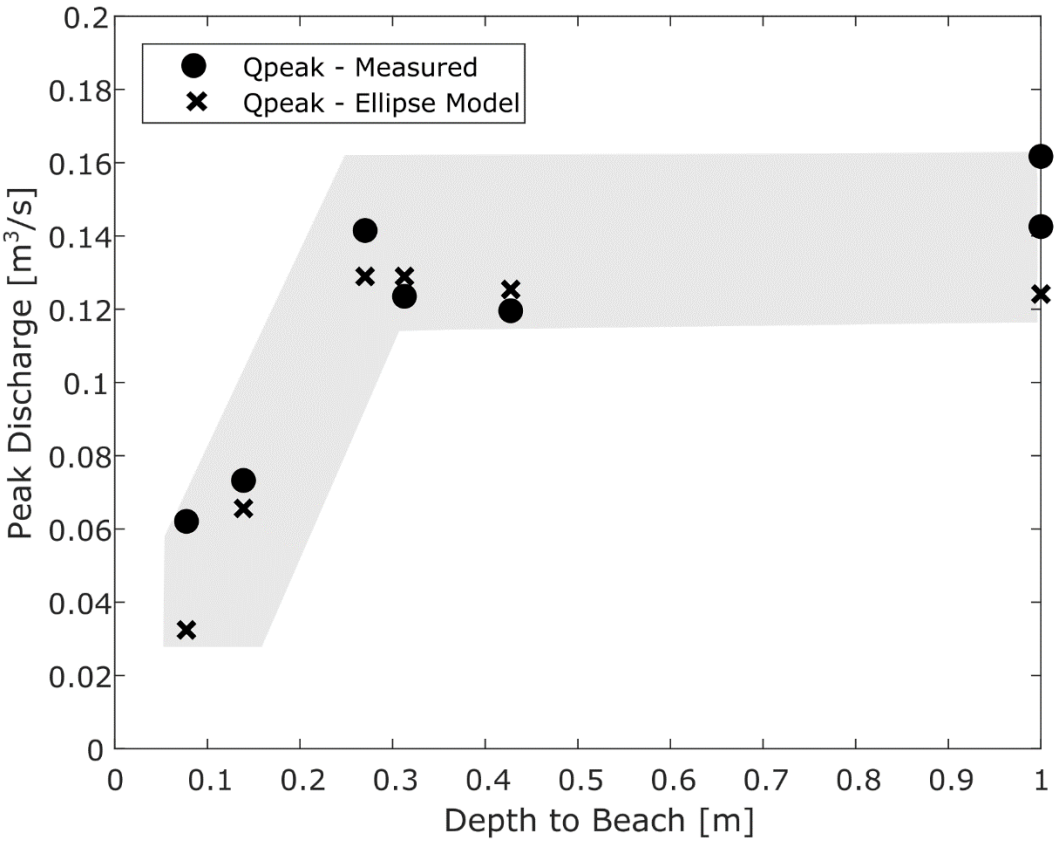

Figure 3.12: Peak discharge estimated with semi-ellipse model compared to depth to the beach from maximum pre-breach reservoir elevation. The bounded grey area illustrates the bounds of values measured and estimated. When the depth to beach exceeds approximately 0.25 m, peak discharge was unaffected by the presence of the beach in the reservoir.

Chapter 4

Conclusions

4.1 Summary of Research

An experimental program was conducted to quantify the effect of upstream geometry on peak discharge in the overtopping failure of tailings dams. Two test series investigating the breach of 1 m high dams were undertaken with the specific objectives of evaluating the influence of dam upstream slope angle on peak discharge for water retaining dams, to quantify the breach crest's control on discharge throughout failure, and to understand the conditions in which a shallowly sloping tailings-style beach in the upstream reservoir impacts peak discharge.

In the first test series, presented in Chapter 2, six dams were constructed with an upstream slope angle ranging between 10.0° to 30.0° from horizontal. The downstream slope of 18.4° and breach crest width of 0.30 m were maintained in each test. Each dam in this research project was constructed with the same homogenous, fine grained sand, and breach was initiated in all tests by incising a v-notch in the centre of the dam crest, causing overtopping. The dynamic geometry of the erosional breach crest feature was measured with high-resolution images, allowing for the shape to be assessed in a mathematical framework of a semi-ellipse. To aid in delineation of the breach crest shape, a thin layer of black sand was placed on the upstream slope of the dam, permitting the definition of the surface elevation of the erosional breach crest feature. The reservoir elevation was monitored with a series of wave capacitance gauges, from which discharge could be calculated as a function of reservoir geometry.

The second test series, presented in Chapter 3, included the addition of shallowly sloping beaches to the reservoir, extending upstream from the dam face at a slope of 2.9° (5%). Beach height,

measured from the flume base to the upstream slope intersection, ranged from 0.50 m to 0.90 m. The upstream dam slope was held constant at 18.4° in each of these tests. Similar to the first test series, instrumentation was utilized to measure breach crest shape evolution and discharge rates.

4.2 Conclusions

The following conclusions were made from the two physical model test series, with a combined total of 11 test dams, focused on the objectives of utilizing a mathematical framework to define the upstream breach crest evolution and quantifying the effect of upstream geometry on peak discharge during overtopping breach in tailings dams.

The shape of the breach crest was demonstrated to be semi-elliptical throughout failure, which formed the basis of the mathematical framework presented to numerically calculate peak discharge for a variety of upstream geometries. The breach crest growth rate, for both B and B*, was shown to be linear from the onset of morphological Stage 3, defined as the time datum, to the time of peak discharge. The aspect ratio of the elliptical breach crest shape was also observed to be relatively stable during this period. The effect of the upstream slope angle on peak discharge, which was observed to be linearly correlated, could then be quantified for a range of slope angles, concluding that due to greater depth between the reservoir surface and the upstream slope of the dam, steeper upstream slope angles resulted in higher peak discharge for dams with similarly sized reservoirs.

In Chapter 3, the presence of a shallowly sloping beach in the upstream reservoir was investigated. The results of this test series were utilized to quantitatively confirm that a beach may only impact peak discharge if the breach crest intersects the beach slope prior to reaching peak discharge on the outflow hydrograph. Test data showed that peak discharge was reduced by up to 50%, from 0.14 m^3/s to less than 0.07 m^3/s when beach heights were greater than or equal to 0.80 m. Peak discharge

was unaffected in tests conducted with beach heights up to 0.72 m when compared to tests with no beach and a similar dam upstream slope angle from Chapter 2.

4.3 Future Work

The work conducted as part of this research project was constrained to the case of overtopping in homogenous, noncohesive dams, where materials did not experience liquefaction during failure. Other failure modes, such as shear failure, are anticipated to effect the breach outflow hydrograph, and should be the subject of future physical model tests. Additionally, static liquefaction of tailings materials is of concern to dam owners and engineers due to observed liquefaction during breach events (Fourie et al., 2019), which may impact the outflow hydrograph and effect rheological conditions of the breach flow. Triaxial testing of test model construction materials should be undertaken to establish the critical state line, required to understand conditions necessary to for liquefaction to occur in the context of critical state soil mechanics framework (Jefferies & Been, 2016). To date, tailings materials from a mine mineral processing mill have not been utilized in dam breach physical model testing. However, these anthropogenic materials may behave differently than naturally occurring materials of similar grain size, and should investigated (Reid & Jefferies, 2017).

Future studies could measure flow velocity at the breach crest utilizing particle image velocimetry or in stream acoustic velocimeters. This data could be used to directly calculate the Froude number at the breach crest and compare to the results of Walder et al., 2015. Scale effects of the dam height should be explored by constructing both shorter and taller dams, and/or conducting tests in an increased gravity environment in a geotechnical centrifuge. Finally, enhanced density control during construction and block sampling could improve the quality of the data. Further studies should be conducted to assess any coupled effects of increased dam density with respect to upstream slope angle.

4.4 References

Fourie, A., Reid, D., Russell, A., Rahman, M., Vinod, J., & Vo, T. (2019). Static Liquefaction of Tailings : An Update on the Industry-Funded TAILLIQ Research Project. In J. Goodwill, D. Van Zyl, & M. Davies (Eds.), *Proceedings of Tailings and Mine Waste 2019 Conference* (pp. 543–554).

Jefferies, M., & Been, K. (2016). *Soil Liquefaction: A Critical State Approach* (2nd Editio). Boca Raton, Flordia: Taylor & Francis Group.

Reid, D., & Jefferies, M. (2017). State Parameter as a Geological Principle in Tailings. *Proceedings of Tailings and Mine Waste 2017 Conference*. Banff, Alberta.

Appendix A

Density Tests

Date	Test ID	Measured Dry Density (kg/m3)				Measured Water Content (%)			
		EC	MC	WC	DS	EC	MC	WC	DS
20181017	S2	1552	1507	1547	1513	2.88	2.53	2.24	8.10
20181211	S3	1512	1468	1483	1556	2.11	2.09	2.08	13.99
20190205	W1	1460	1428	1508	1548	1.00	1.00	1.06	4.54
20190305	W2	1442	1478	1491	1549	2.16	1.60	1.97	8.57
20190403	W3	1559	1555	1547	1499	2.76	2.89	2.75	11.62
20190413	W4	1509	1478	1484	1591	1.75	2.03	1.77	17.55
20190503	W5	1463	1458	1486	1632	2.54	1.89	1.98	16.34
20190522	S4	1519	1480	1534	1511	7.19	5.00	5.33	9.58
20190530	S5	1535	1528	1500	1569	2.92	3.20	3.01	11.14
20190606	S6	1535	1473	1536	1658	1.46	1.82	1.92	13.98

Test Locations

EC: East Crest

MC: Middle Crest

WC: West Crest

DS: 1 m downstream of crest, on dam centre line